3-21-2013

Computational Simulation of Explosively Generated Pulsed Power Devices

Mollie C. Drumm

COMPUTATIONAL SIMULATION OF EXPLOSIVELY GENERATED PULSED POWER DEVICES

THESIS

Mollie C. Drumm, Captain, USAF

AFIT-ENY-13-M-11

DEPARTMENT OF THE AIR FORCE
AIR UNIVERSITY

AIR FORCE INSTITUTE OF TECHNOLOGY

Wright-Patterson Air Force Base, Ohio

AFIT-ENY-13-M-11

COMPUTATIONAL SIMULATION OF EXPLOSIVELY GENERATED PULSED POWER DEVICES

THESIS

Presented to the Faculty

Department of Aeronautical Engineering

Graduate School of Engineering and Management

Air Force Institute of Technology

Air University

Air Education and Training Command

in Partial Fulfillment of the Requirements for the

Degree of Master of Science in Aeronautical Engineering

Mollie C. Drumm, BS

Captain, USAF

March 2013

AFIT-ENY-13-M-11

COMPUTATIONAL SIMULATION OF EXPLOSIVELY GENERATED PULSED POWER DEVICES

Mollie C. Drumm, BS
Captain, USAF

Approved:

Dr. Robert B. Greendyke (Chairman)	Date
Capt. David Liu (Member)	Date
Capt. Christopher L. Martin (Member)	Date

Abstract

Technology and size constraints have limited the development of the end game mechanisms of today's modern military weapons. A smaller, more efficient means of powering these devices is needed, and explosive pulsed power devices could be that answer. Potential advancement opportunities exist with the growing field of research that surrounds explosive pulsed power devices. While most of the research to date has been in the experimental field, if these devices are going to be a viable option for use in future weapon development, there is a genuine need for more theory-based research and an accurate computer modeling capability. One of the programs that has done much experimental work with ferroelectric generators (FEG) is the US Army at Redstone Arsenal in Huntsville, Alabama. The objective of this research was to use the Redstone experimental data collected from an FEG of their own design in combination with the ALEGRA-EMMA code, a hydrodynamic code developed by Sandia National Laboratories, to develop a computer model that can accurately represent an FEG and that can be verified against existing experimental data and eventually used to predict future experiments. Three experimental scenarios were used from the existing collected data: an FEG wired into an open circuit, an FEG wired into an 8-blasting cap circuit, and an FEG wired into a 64-blasting cap circuit. The three areas of this research that had to be explored simultaneously were developing an accurate model for the ferroelectric material, developing an accurate model to represent the external circuit load, and recreating the Redstone FEG design in the ALEGRA computer environment. Once these three aspects were covered and the overall model was developed, the individual cases for each scenario were run in the simulation model. The simulation results were compared to the respective ex-

perimental data, both current and voltage, and the model was evaluated. While the ALEGRA code is not capable of simulating the breakdown phenomenon seen in the open circuit cases, the model can accurately reproduce the peak values for the current but has problems reproducing the peak values for the voltage for both the 8-blasting cap and 64-blasting cap scenarios. The model also fairly accurately reproduces the general shape of the current and voltage data in both scenarios as well, though the time scale of the simulation reaction is slightly shortened from the time scale seen in the experimental data. Overall, the developed model provides a good baseline simulation capability that can be used as a springboard for future development with further research. Being able to advance this baseline for use with FEG design optimization can eventually result in growth and development for future weapons, an area that should be constantly improving in order to keep the United States Air Force on the cutting edge of technology.

Acknowledgements

First I would like to thank my research advisor, Dr. Robert Greendyke for all of his time and effort in guiding my research. His insight has proved to be a great addition to my thesis and to my overall academic experience and development.

Secondly, I would like to thank my thesis committee members, Capt Chris Martin and Capt Dave Liu, for their input and comments on my thesis. Their help was instrumental in creating a worthy thesis.

Next I would like to thank Mr. Allen Stults and Dr. Larry Altgilbers from the U.S. Army Aviation and Missile Research, Engineering and Development Center. Their patience with me as I learned throughout this process was immense, and they took care to provide me with anything needed through the course of this research.

Last, but certainly not least, I would like to thank Mike Wong from Sandia National Laboratory for his help in training me in the use of the ALEGRA codes and in helping me develop my input files. His willingness to help thoroughly answer every question I could think of is what gave this research the jumpstart that it needed to put me ahead of the game.

Mollie C. Drumm

Table of Contents

List of Figures

List of Tables

COMPUTATIONAL SIMULATION OF EXPLOSIVELY GENERATED PULSED POWER DEVICES

I. Introduction

1.1 Motivation and Background

Modern military weapons have hit a plateau in their development. While there has been advancement in the acquisition and targeting steps of the kill chain, the actual end game kill mechanism is stuck in an older realm of third generation technology. Size constraints and, to some extent, technology limitations have potentially stunted the growth of what should be one of the important areas of focus in research and development due to increasing dependancy of militaries on electronics. Ideas such as directed energy (DE) and electromagnetic pulse (EMP) could provide great advantage in operational capabilities over traditional kinetic solutions, both in lethal and non-lethal weapons, but they suffer from implementation issues in the form of size and cost. With the growing need for smaller, more efficient means of powering new technology, the idea of a compact, self-contained power source capable of generating high electrical power output is an ideal solution. Explosive pulsed power (EPP) generators could be that solution.

The concept of explosive pulsed power generation has been studied since the 1950s and the technology has been explored mostly through the avenue of experiment, though it is only recently in the last 15 years that this field has again come to the forefront of study (5). Born out of the nuclear programs in the US, UK and Soviet Union, researchers were looking for a way to replace fission bombs to achieve fusion

in the hydrogen bomb and believed this could be accomplished with pulsed power generators (6). Explosive pulsed power devices offer a compact, stand-alone system that produces high-yield power output in proportion to their size. There are five general classes of EPPs, but three are most suited to practical applications. These are the magnetic flux compression generators (FCG), ferromagnetic generators (FMG) and ferroelectric generators (FEG). The first device works on the concept of field interaction between a conducting medium and a magnetic field. The last two devices make use of either magnetic or electric fields stored in a prepared material (4).

This research will focus on the ferroelectric generator as a high voltage source for practical applications. An FEG operates by utilizing the stored chemical energy in a small amount of high explosive (HE) to propagate a shock wave through a block of polarized ferroelectric material, thereby releasing the stored energy in that material and converting it to an electrical energy pulse. The most effective, and currently most studied, ferroelectric material in use is lead zirconate titanate (PZT). The shock wave propagating through the block induces a phase change in the crystalline structure of the material that produces a short, high voltage pulse across circuit terminals that are connected to the PZT block. This output pulse becomes an efficient means of short-duration power generation.

Ferroelectric generators as a power source provide a way to drive these advanced weapons discussed earlier while minimizing both space and weight. Commercially available FEGs are small enough to fit in the palm of a hand, but the circuit load that could be powered with these devices could vary anywhere from high power microwaves to small directed energy lasers to small EMP devices that can be used to strike localized targets with precision. Their small size could even allow for weapons that can potentially be man portable but still provide enough energy to effectively accomplish the mission.

The United States Army at Redstone Arsenal in Huntsville, Alabama has been conducting experiments with FEGs over the past several years totaling 27 tests and has an extensive compilation of these experimental results. Although there are several companies that produce commercially available FEGs, testing was accomplished utilizing an FEG that was designed and constructed at Redstone. The details of this design and experimental results will be discussed in Chapter II of this document. The experimental arrangements that were tested include an FEG connected to an open circuit and an FEG connected to an inductance load. The inductance load was varied in the form of set numbers of commercial blasting caps wired in series in the circuit. The number of blasting caps was varied between 8 and 128, and the inductance load was measured for each test in microHenries (μH). The time history of the output pulse was captured for each test.

This catalog of results serves as the foundation for this research. While all of this technical data on the operation and output of FEGs does exist, there is a gap in the knowledge database. There is a need to be able to computationally model the inner workings of an FEG and to predict this voltage output. The ability to accurately model these generators would allow for expanded research opportunities. Additionally, the capability to optimize a design for a required use while decreasing the system cost facilitates a faster progression towards incorporating these devices into advanced weaponry and moves ideas from the laboratory into the hands of those that need them on the front lines.

1.2 Research Objective

The fundamental objective is to determine if it is possible to accurately model the operation of the Redstone FEG in multiple experimental circuit load configurations and reproduce the current and voltage time histories for several of the tests. This

will be accomplished by building a computer model using the ALEGRA-EMMA code developed by Sandia National Laboratories (SNL) that can be used to capture the operation and electrical pulse of an FEG. The ALEGRA code is a multi-material, multi-physics hydrocode that can be used to model high-speed shock physics and solid dynamics. The use of the ALEGRA-EMMA code will also be discussed in detail in Chapter II. The initial attempt will be made to recreate the scenarios that were used in the experimental testing at Redstone with the global goal of a developing a model that can be adapted for predictive operations, which will be done in two steps. The first step is to adapt the ferroelectric model provided by SNL so that it accurately represents the PZT material that was used in testing. The second step is to use circuit theory to recreate a circuit model that represents the electric load that was used in experimental testing. Through the course of the research, the model output data will be correlated with existing experimental data to demonstrate and validate the models ability to accurately portray the physics of explosive pulsed power devices and its potential for prediction of future experimental results.

II. Background

2.1 Chapter Overview

This section will discuss the field of pulsed power generation and its progression to this point in time. It will include a description of pulsed power devices, specifically FEGs and their uses. It will also discuss results from experiments that have been conducted and their implications in this research. An overview and explanation of the ALEGRA-EMMA code produced by Sandia National Laboratories is also presented as well as an account of what this code brings to the research.

2.2 Pulsed Power Devices

In the broadest sense, pulsed power devices are those devices that convert stored chemical energy to electrical energy which is accomplished through the use of HE to drive the reactions that release the stored energy. The subset of this category of devices that this research is concerned with is the FEG. This type of generator works specifically by using shock waves from HE detonation to induce a crystalline structure phase change in a block of polarized ferroelectric material. The ferroelectric ceramic material is the key to the operation of this type of device.

Ferroelectric Materials

The background first begins with a discussion on ferroelectric and piezoelectric material. All dielectric materials share the general ability to mechanically change their shape by reorienting their molecules under an applied external electric field, called electrostriction. Once the electric field is removed, the material retains its distorted shape and has a residual strain. It is said to now be a polarized material. A subset of these materials, ones that have a crystalline structure, can have a piezoelectric

property. Piezoelectricity in materials is similar to the process of electrostriction, where under an applied mechanical stress they develop an electrical polarization (8).

Several of these types of materials also have the characteristic of a permanent dipole moment and a specific polar axis, even with no external stress or external electric field applied. The effect is termed spontaneous polarization, though is not spontaneous in the literal sense. This group is referred to as pyroelectric materials, called as such for the polarization magnitudes dependence on temperature.

An even smaller subset of the pyroelectric group of materials is a class of crystalline materials called ferroelectrics. These materials are categorized by having at least two orientations for the spontaneous polarization vector and the ability to switch between these orientations when an external electric field is present. For an FEG, the polarization property that is most important is the remnant polarization that remains when the electric field is removed after the substance has been poled to its peak value or its spontaneous polarization (6). The remnant polarization is the stored potential of electrical energy that will be released when the material is impacted by the explosive shock wave. As the electric field is applied to the material it follows one polarization path and reaches the spontaneous polarization. As the field is removed it relaxes along a different path, a hysteresis effect, which can be seen in Figure 1. The remaining polarization once the electric field relaxes back to zero is the remnant value. The ratio of the remnant polarization to the maximum spontaneous polarization is the saturation, a percentage value that is effectively how well the material holds the applied polarization.

Another important aspect of ferroelectric materials is the difference between ferroelectric (FE) states and antiferroelectric (AFE) states of the material structure. It is feasible that there could be areas of the material where cell dipoles are aligned with one of the axes and areas where cell dipoles are aligned oppositely. The similarly

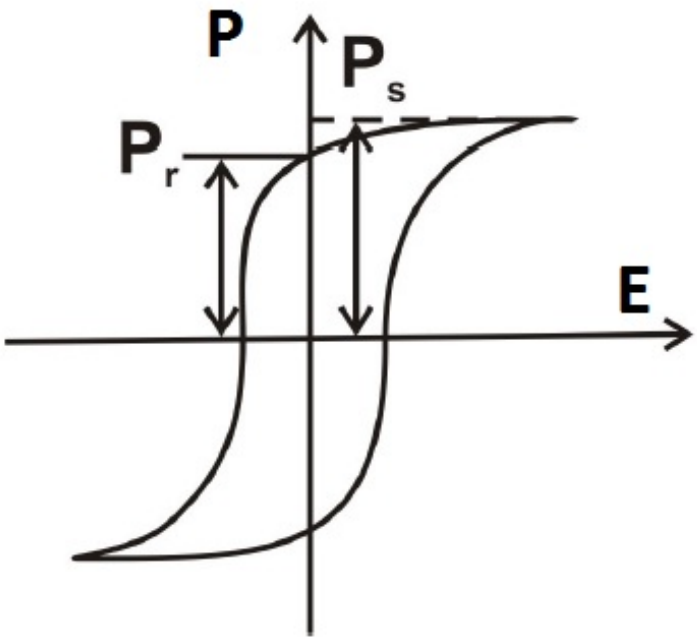

Figure 1. Shows the polarization curve and hysteresis effect that occurs when applying an electric field to a ferroelectric material. The spontaneous polarization (Ps) is the peak value of polarization that can be reached. The remnant polarization (Pr) is the value left when the electric field is relaxed to zero. (1)

oriented cells form domains of polarization. If the number of domains aligned with one axis are approximately the same as the number aligned oppositely, it results in a zero net polarization and the material is called antiferroelectric. If on the other hand the cell dipole moments all align in the same direction, it gives rise to the ferroelectric state where there does exist a maximum net polarization on the material. An applied stressor, whether it is mechanical or electrical, can cause the transition between these two states in either direction (i.e., from ferroelectric to antiferroelectric and vice versa). The operation of the FEG makes use of the transition from ferroelectric into the antiferroelectric state to release the stored electrical potential energy, thus providing the electrical output pulse. The rate at which the material transitions from ferroelectric to antiferroelectric state is called the phase transition rate.

Dielectric materials also have a dielectric constant, which is the ratio of the permittivity of the material to that of a vacuum. The permittivity of the ferroelectric essentially relates to its ability to polarize in the presence of an electric field, which reduces the field inside the material. In the case of an FEG, the permittivity is a relation of the capacitance of the ferroelectric material (6). The capacitance will affect the how the FEG interacts with the circuit load, and thus the permittivity has a great impact on the output response of the FEG. Since ferroelectric materials essentially have two states, they also have a permittivity for each state (i.e., a ferroelectric permittivity and an antiferroelectric permittivity). Permittivity is a measured property that is experimentally determined. Thus, it is fairly easy to determine for the ferroelectric state of a material. However, it is more difficult to determine for the transitioned antiferroelectric state and is usually an estimated value at best.

By far the most tested ferroelectric ceramic material and most suitable, and therefore most widely used, is lead-zirconate-titanate or PZT, specifically PZT 95/5 ($Pb(Zr_{0.95}Ti_{0.05})O_3$). The suitability and efficiency of PZT 95/5 comes from the fact

that in its polarized FE state, PZT 95/5 sits very close to a phase boundary between FE and AFE, and the hydrostatic pressure from a shock wave is enough to force the material across the boundary into the AFE state, completely depolarizing it. The PZT material can be cut and manufactured in many different shapes and sizes. Rectangular, cylindrical, conic and ring shapes are common forms that are used in some commercial FEGs. The shape used for this research is a small rectangular block shape that will described in later sections. Shape versatility allows the manufacturer and user to also control the direction of the polarization vector, which is an important aspect since direction of polarization directly affects the pulse output levels from the PZT. There are two directions for the block shape: transverse and longitudinal. Once installed in an FEG, a polarization vector that is perpendicular to the shock wave propagation direction is called a transversely polarized FEG. A polarization vector that is parallel to the direction of propagation is called a longitudinaly polarized FEG.

FEG Operation

Now that the background on ferroelectric materials has been covered, the next subject is the internal operations of an FEG and how an electrical pulse is produced. There are several variations on the design of an FEG, but the principle of operation is the same in all of them. The ferroelectric material is secured in the generator structure in either the transverse or longitudinal polarization direction, depending on the desired output. A small amount of high explosive is detonated, producing a shock wave front that propagates in the direction of the PZT block. The shock wave will depolarize the PZT block, releasing the stored polarization (i.e., charge that remained as a result of the remnant polarization), and transition the phase from the ferroelectric to the antiferroelectric state. The charge release causes an output current and/or voltage, with peak values that change based on the PZT parameters

and depending on the circuit load that is attached to the FEG.

Electrical leads are attached to opposing sides of the PZT block in order to create a positive and a negative terminal, the difference being determined by the polarization vector of the PZT block. These terminals can be connected by wire leads to any type of electrical circuit load that a user desires. The terminals act the same as the positive and negative terminals of a battery, where once the PZT starts its phase transition, a voltage and current are provided to the circuit load.

In order to obtain the maximum effectiveness from the PZT, a planar wave front is desired in order to uniformly depolarize the PZT material. In some designs, there is a structural guide that shapes the shock wave into a planar front rather than the spherical shock wave front that naturally propagates. In other designs, there is a very thin, curved metallic plate, usually copper, that acts as a flyer plate. The curved shock wave from the explosive impacts that shaped metallic plate and deforms it and moves it across a small void between the plate and PZT to impact the PZT block in such a way as to create a uniform planar impact wave. Both methods achieve the desired result of a uniform phase transition through the ferroelectric material. In designs that do not include a mechanism to induce a planar wave front, a peaking switch is included in the design. The switch connects the wire leads of the circuit in an initial open circuit configuration and allows the current and voltage to build up to its peak value before breaking through a thin dielectric material and allowing the switch to close the circuit, producing the highest peak in the shortest time.

All of the materials of the FEG assembly are held together by a potting material and in some designs a plastic housing case that helps maintain the integrity of the assembly through the shock wave propagation. The potting material surrounds the block of PZT but should not itself participate in the electrical circuit portion of the FEG output. Therefore the potting material must be chosen carefully. If the

assembly is not held together through the entire PZT phase transition, the circuit will be broken, and the full potential of the FEG will not be utilized.

Breakdown Mechanisms

The failure mechanism associated with FEGs is called electrical breakdown, an important phenomenon that occurs within the ferroelectric material under the applied stress of an external electric field that essentially causes the circuit to break. Breakdown is a very complex occurance that greatly affects the power output ability of the ferroelectric material. There are three types of breakdown mechanisms that can occur in a ferroelectric material: intrinsic, thermal and discharge breakdown. All three result in large current flows that have the same damaging effect on the overall operation.

Intrinsic breakdown occurs when the applied electric field strength is large enough to provide sufficient kinetic energy to free electrons participating in the reactions so as to ionize neighboring atoms. It is generally agreed that this is accomplished through electron impact ionization. The process adds more electrons to the reactions, thereby perpetuating the events, ultimately resulting in a large current flow and a catastrophic failure mechanism.

Thermal breakdown is more a characteristic of the thermal properties of a dielectric material. If the electric field is strong enough to produce excessive heating that cannot be adequately dissipated by the material, it can lead to increased conductivity and dielectric strength loss. Like the previous breakdown mechanism, the process, once started, can perpetuate itself to the point where it results in breakdown failure.

The final failure mechanism, discharge breakdown, is slightly less understood as to how it occurs, but it is linked to the material property of porosity. The inhomogeneity due to porosity can lead to pockets of non-uniform electric field strength throughout

the material. Specifically, within material pores, the electric field strength can be much stronger, leading to a discharge occuring within a single pore. Debate exists as to how these pore discharges lead to material breakdown, but several theories include the possiblity of increased electric stress, increased mechanical stress, or possibly increased heat generation (8).

In reality, the intrinsic and discharge breakdown are the most common failure mechanisms that are seen with the operation of FEGs and their associated ferroelectric ceramics. The complex nature of these mechanisms leads to having very little in the way of mathematical theory to physically describe and predict how dielectric ceramics will fail in a breakdown, which makes modeling breakdown a challenging subject, but there does exist experimentally observed results than can correlate these phenomena to physical properties. The dielectric strength refers to the maximum electric field that the material can withstand without suffering breakdown. The dielectric strength can also be experimentally determined and is very dependent on the specifics of the material to include size, shape, material defects.

In a study that looked at the breakdown of longitudinally shocked ferroelectric ceramic materials (14), the authors performed several experiments that showed evidence of breakdown effects that significantly alter the voltage output that is seen from the shocked ceramics. Both mechanical failure as well as increased conductivity and corresponding current leakage were discussed and ruled out as causal factors, thus leaving electrical breakdown as the culprit. The authors use the gathered experimental data to correlate the breakdown electric field strength to the ceramic sample disc thickness. The reader will be able to see evidence of this type of electrical breakdown phenomena in the discussion of the the previous experimental results that are below.

2.3 Previous Research

Previous research in the area of ferroelectrics and FEGs started in the 1950s with government programs supporting nuclear weapons programs. One of the branches being explored in this area was different "primaries" (i.e., different ways to achieve detonation of the secondary main fuel of a nuclear bomb). The requirement for a primary is the ability to heat the main fuel to the point where fission can be achieved. The two main systems being researched were lasers and pulsed power devices. The benefit of pulsed power is that a smaller amount of contained energy can be generated over a relatively large amount of time and stored, then released over a much smaller fraction of the time to increase the peak value of the output pulse. A pulse keeps the total stored energy the same, but generates an impulse that significantly amplifies the achievable output values.

Development was independently being done in multiple countries, in particularly the United States and the Soviet Union. Research started with developing non-explosive pulsed power systems. High-voltage pulsed power systems were studied in the 1960s in England, using capacitor banks and Marx generators (a specific design of capacitor bank) to charge transmission lines with voltage pulses (6). These types of systems continue in use in scientific endeavors today, but while these types of systems provide all the benefits of pulsed power, the area in which they suffer is in size. The systems of capacitor banks and Marx generators can range from the size of trucks to rooms in a building. There is very little chance of a portable system in this case, which is where the idea of an explosive pulsed power system, with its much smaller size, is very appealing and why the idea gained momentum with the research community.

Most of the research in the area of explosive pulsed power has been predominately experimental. Other than basic operating knowledge, it has been phenomenally easier

to collect experimental data and anaylze than to delve into the theoretical basis. There has been no need to look further when experimental data provided information that was good enough for intended uses. It is only recently that an interest has developed in exploring the physics behind the operation of these devices in order to more accurately characterize output.

In order to start characterizing output, the most important area to look at is the ferroelectric material itself and its behavior under dynamic conditions. Shock wave propagation through a solid material is fairly well understood through gathered empirical data, but the interaction with the ferroelectric material needed much further study. One of the most applicable areas of previous research is a series of experiments that was conducted by researchers at Sandia National Laboratories looking at the mechanical and electromechanical changes that are undergone by the ferroceramic PZT when compressed by shock waves. Specifically, researchers were looking at $Pb_{0.99}(Zr_{0.95}Ti_{0.05})_{0.98}Nb_{0.02}O_3$, a variant of PZT 95/5 that has been doped with 2 percent Niobium. The set of experiments that was conducted was part of the more recent upswing in the research into FEGs and ferroelectric ceramics. A strong interest in being able to model the inner workings of an FEG was developing, and these studies were performed in an effort to characterize and improve the dynamic material model for ferroelectric ceramics. A series of several papers were written conveying the results from these experiments. Two of the most useful to this research were written on the topics of determining the Hugoniot states and mechanical properties of the material and the shock-induced depoling characteristics (12; 13). Although the PZT studied in this set of experiments was not the same formulation as that used in the experiments conducted at Redstone, the general trends that were seen in the results can be applied to this current research topic in being able to accurately model the Redstone PZT material.

As stated above, it is only recently that there has been a desire to be able to computationaly model EPP devices, specifically FEGs. Sandia National Laboratories has been working on research in this area since the 1990's, but funding issues delayed a full product from being developed which is where the development of the ALEGRA-EMMA code, described below, began. The computer code capability married with the study of the PZT properties is what is required in order to pursue this line of research.

2.4 Previous Experimental Results

Mr. Allen Stults, Mr. David Clark and Mr. Robert Hartleben with the United States Army at the Aviation and Missile Research, Development, and Engineering Center in Redstone, Alabama have conducted well over 400 tests with an FEG of their own design (15). Graphical results for 22 of these tests have been provided for comparison to computational simulation output. The Redstone design functions under the same main theory of FEG operations. A block of four grams of C4 high explosive is packed into a plane wave generator, a plastic triangular prism shape that is aptly named as it is designed to manipulate the shock wave produced upon detonation so that once the shock wave reaches the end of the shape and the C4 has completely detonated, the shock wave front will essentially be planar. The design attempts to ensure that the wave front will hit the thin copper plate that is adjacent to the plane wave generator piece at approximately the same time across the face of the plate, eliminating the need for a peaking switch in this design. The shock wave propagates through the copper plate and into the potting material that surrounds a block of PZT 95/5 that is manufactured by TRS technologies. The PZT block and potting material are held in place by a plastic housing case. The housing case, copper plate and plane wave generator are all bolted together. The PZT block is 2.0 by 0.5

by 0.5 inches, with the longest side oriented perpendicular to the direction of wave propagation. The PZT is polarized in the transverse direction. The front (positive terminal) and back (negative terminal) face of the PZT block are prepared with high voltage wire leads fixed to electrodes on the surface. The design also has the option of including a capacitor between the positive and negative terminals (see Appendix A for engineering schematic drawings). Figure 2 shows three views of the Redstone FEG design as photographed during the experiments conducted at Redstone Arsenal.

In some of the experiments, the FEG was placed into an explosive containment tank at the facilities at Redstone Arsenal in Huntsville, Alabama. In other experiments, the tests were conducted outside in open air. A high-voltage probe and a current meter were attached to the wire of the positive terminal of the PZT block. From here, testing was accomplished for two arrangements: the first, firing the FEG while attached to an open circuit load and second, firing while attached to an inductance/resistance load pair. The data analysis on the provided experimental data was done using a plot digitizer program and MATLAB®. Peak value is the found as the maximum absolute value achieved in the current and voltage plots (or the time where known breakdown occured). Rise time was calculated as the difference in time between the start of the change of the curve and the time that the peak value is reached.

Open Circuit

There were six tests accomplished with the FEG connected to an open circuit load. Two of these tests were conducted with the optional capacitor included in the FEG design, and four were run without the capacitor. In this setup, the positive terminal was connected to the high-voltage probe and the negative terminal was not connected to any load, making this an open circuit. Table 1 below summarizes the results from

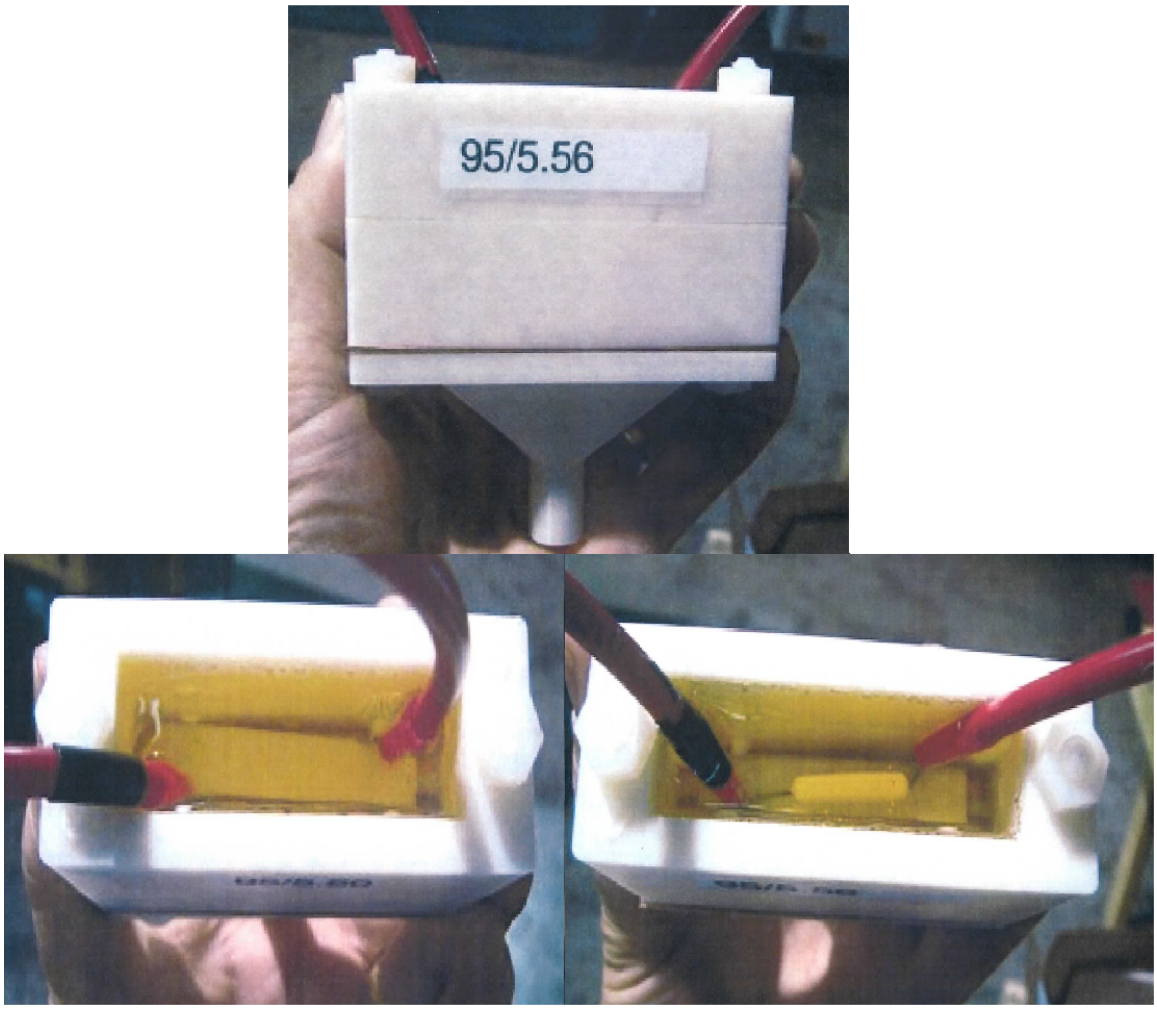

Figure 2. Top photograph shows an external view of the outside housing of the Redstone FEG. Lower left photograph shows an internal view of the PZT block without the internal capacitor. Lower right photograph shows an internal view of the PZT block that includes the internal capacitor.

these runs, to include rise time and peak voltage values. The peak values are the highest value recorded before breakdown occurs. This evidence of breakdown is very similar to what was seen in the studies done by Shkuratov, Talantsev, and Baird (14). There is no current data as the circuit was an open circuit. Any current seen in the experimental data is a result of the current associated with the circuit and measuring devices after PZT breakdown and is therefore not a factor for comparison. Only the experimental tests without the capacitor were considered for this study to get a truly open circuit model. There were four of these tests and Figure 3 through Figure 6 show the voltage data plots collected for these tests. These are the experimental results that will be used to compare against the open circuit simulations.

Table 1. Open Circuit Experimental Results.

Run Number	**Rise Time** μs	**Peak Voltage** V
Test 1	0.6639	32,990
Test 2	0.6329	33,280
Test 3	0.7276	32,000
Test 4	0.8549	51,940

In three of these plots, Case 1 through Case 3, the peak voltage value reached is approximately the same, just below 35,000 volts. The fourth test reaches a higher value of about 52,000 volts before reaching a plateau in the graph for 0.2 microseconds and then suffering breakdown. Even though all four open circuit tests were conducted with the same configuration and PZT formulation, the peak values are not the same for all tests. However it can be seen from looking at a plot of all four tests together on a coincident time axis (Figure 7) that they have essentially the same slope when the voltage starts to rise. The almost identical slope indicates that the reaction rate of the PZT materiel was the same for all of the tests but that the breakdown mechanism did not occur at the same point in time in the reaction.

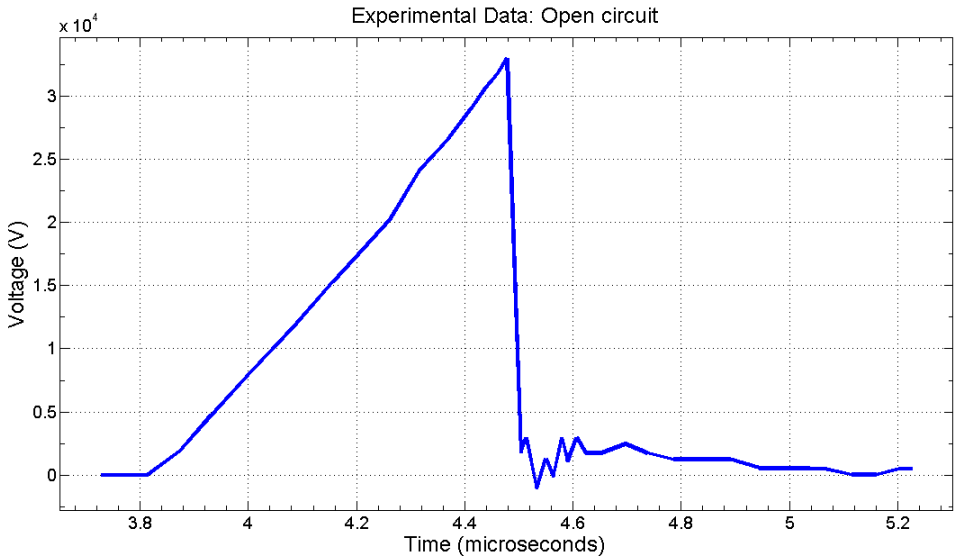

Figure 3. Test 1 - Experimental data consisting of an FEG fired into an open circuit. Test 1 conducted October 27, 2010.

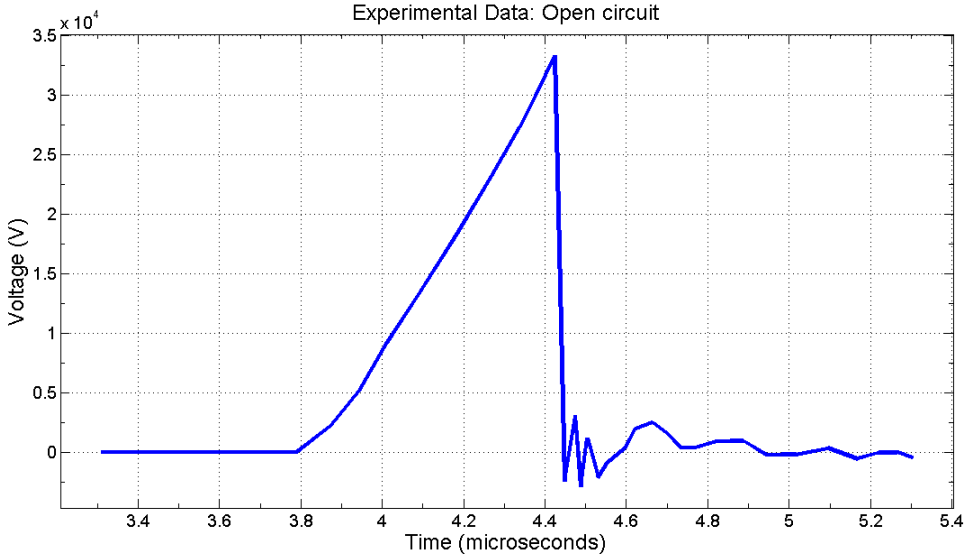

Figure 4. Test 2 - Experimental data consisting of an FEG fired into an open circuit. Test 2 conducted October 27, 2010.

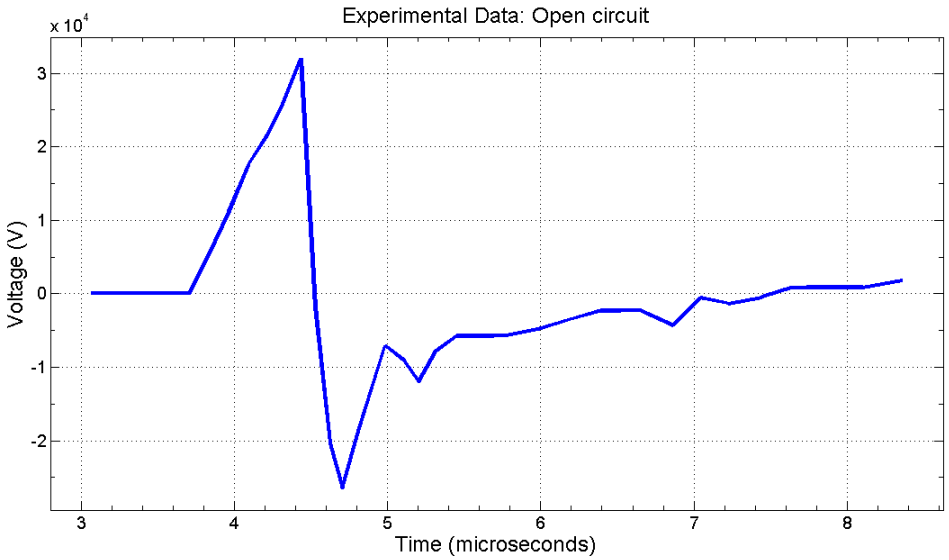

Figure 5. Test 3 - Experimental data consisting of an FEG fired into an open circuit. Test 1 conducted March 9, 2011.

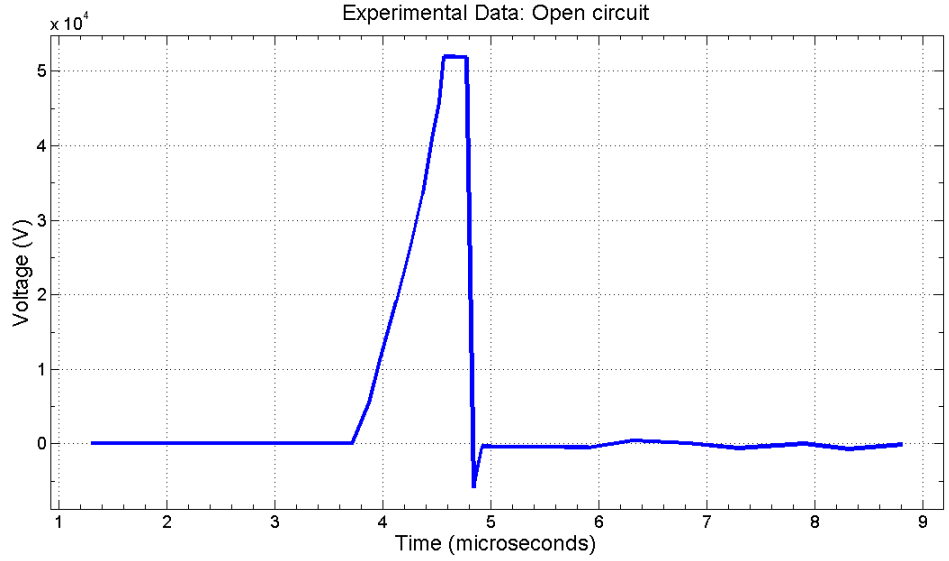

Figure 6. Test 4 - Experimental data consisting of an FEG fired into an open circuit. Test 1 conducted November 16, 2011.

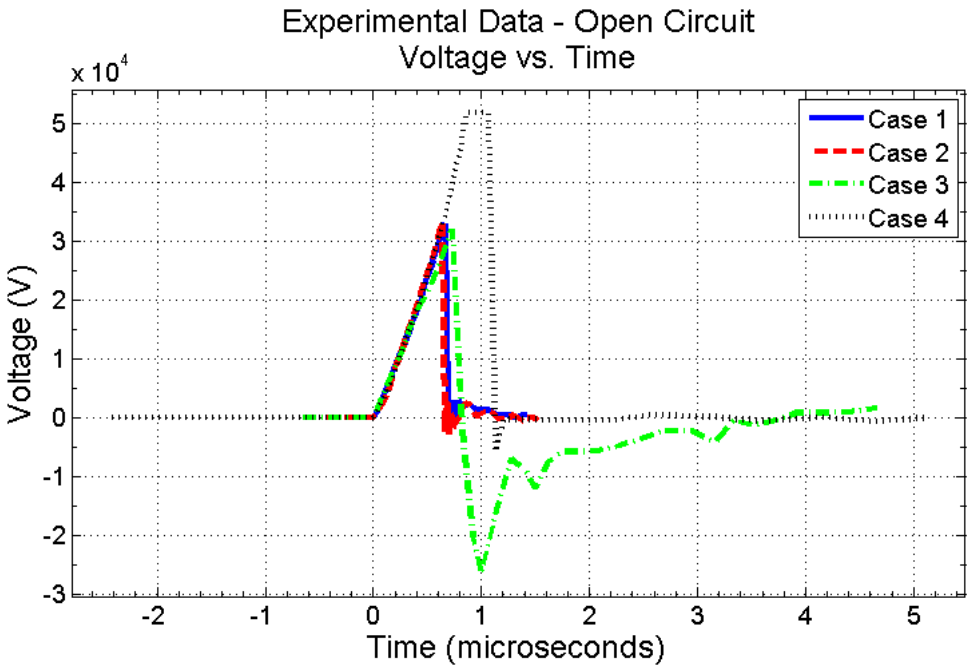

Figure 7. Experimental data showing all four open circuit tests with coincident time axis.

Inductance/Resistance Loaded Circuit

There were 16 tests conducted with the FEG connected to an inductance/resistance load pair. The inductance/resistance load was achieved by wiring commercial blasting caps into the circuit. The blasting caps were connected in a series configuration, and the inductance/resistance load was varied by increasing the number of blasting caps that were in the array. Data was collected for 8, 16, 36, 64 and 128 cap arrays. For the purpose of this research, the 8-blasting cap load and the 64-blasting cap load were studied in detail as these runs had the best documented setup. There were four experiments run with the 8-cap load and three experiments run with the 64-cap load. Table 2 below summarizes the results from these runs, to include peak voltage values for each inductance/resistance value pair. Current data was also collected for each inductance/resistance load pair. Values for peak current value can be found in Table 3.

Table 2. Peak Voltages From Inductance Load.

Run Number	**Inductance** μH	**Resistance** Ω	**Rise Time** μs	**Peak Voltage** $Volts$
8 Cap-Test 1	42.9	15.9	0.3383	7530
8 Cap-Test 2	58.6	16.0	0.4210	8612
8 Cap-Test 3	52.2	15.8	0.3707	7530
8 Cap-Test 4	51.6	15.9	0.3667	7783
64 Cap-Test 1	348.8	115	1.2397	10,380
64 Cap-Test 2	337.8	115	1.0370	15,100
64 Cap-Test 3	354.9	126	0.8992	18,100

Table 3. Peak Current From Inductance Load.

Run Number	**Inductance** μH	**Resistance** Ω	**Rise Time** μs	**Peak Current** $Amps$
8 Cap-Test 1	42.9	15.9	1.9082	-41.84
8 Cap-Test 2	58.6	16.0	1.9141	-42.64
8 Cap-Test 3	52.2	15.8	2.0464	-44.00
8 Cap-Test 4	51.6	15.9	1.8981	-41.41
64 Cap-Test 1	348.8	115	2.0727	41.71
64 Cap-Test 2	337.8	115	1.8786	44.98
64 Cap-Test 3	354.9	126	2.6960	46.47

Plots of the voltage and current curves for each of the 8-blasting cap tests are show below in Figure 8 through Figure 11. From these figures it can be seen that the general shape of the graph for the voltage is three positive-valued peaks, decreasing in absolute amplitude at each subsequent peak followed by three negative-valued peaks that also decrease in absolute amplitude for each subsequent peak. The voltage then returns to a zero value with little to no oscillations. The first positive peak and the first negative peak are approximately the same absolute value in each of the tests. Now looking at the current plots for the four tests, it can be seen that they also follow a general shape trend. Note that the current measured for all four tests was negative, but this is merely a matter of orientation of the PZT during the test setup. For future

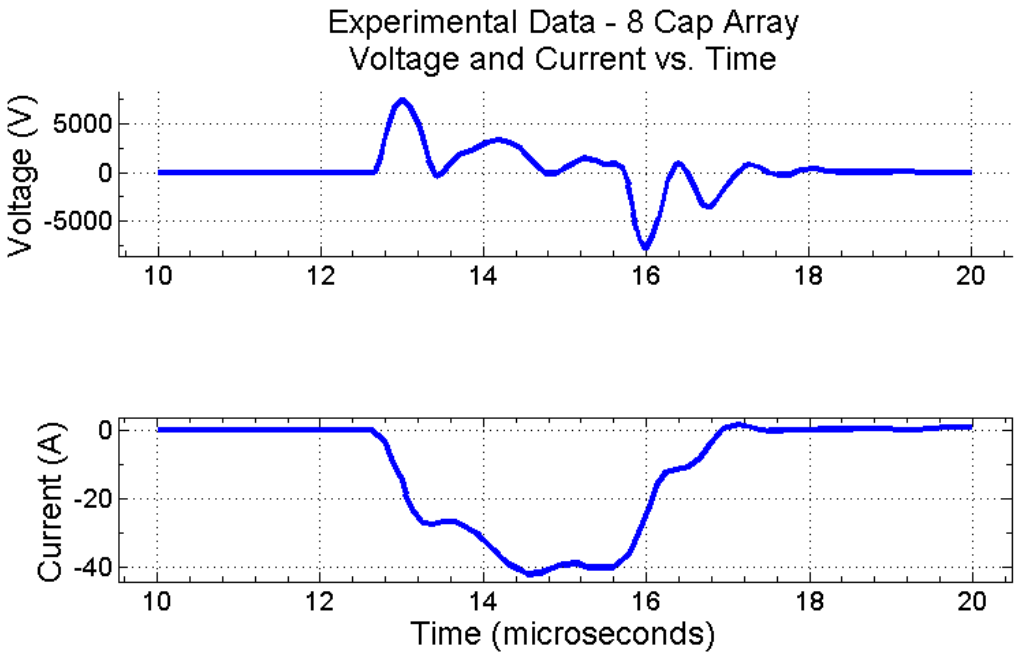

Figure 8. Test 1 - Experimental data consisting of an FEG fired into a circuit with an 8-blasting cap inductance load of 42.9 μH, resistance load of 15.9 ohms and no internal capacitor. Test 1 conducted August 25, 2010.

comparison with simulation results, the data will be kept and shown as provided in the experimental data. In all four test cases, all 8 blasting caps were detonated as a result of firing the FEG.

Looking at the experimental data plotted together with coincident time scales reveals more information as it can be seen that for the four different experiments, not only is the shape of the curves almost identical, but the timing of the rise of the plots for both the voltage and the current are almost identical as are the peak values of the voltage and current. Figure 12 shows this data, which exhibits an experiment with very repeatable results for comparison to simulation data.

Plots of the voltage and current curves for each of the 64-blasting cap tests are shown below in Figure 13 through Figure 15. From these figures it can be seen that these experiments, like the 8-blasting cap arrays, also have similar general shape trends for the current and voltage. Note that the current measured for these cases is

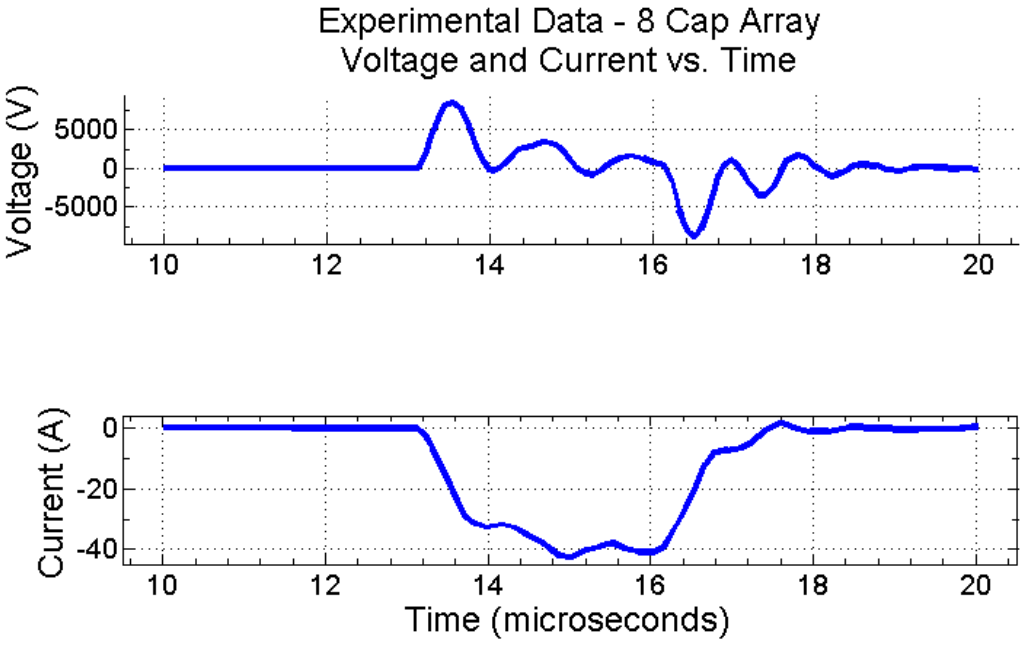

Figure 9. Test 2 - Experimental data consisting of an FEG fired into a circuit with an 8-blasting cap inductance load of 58.6 μH, resistance load of 16.0 ohms and no internal capacitor. Test 2 conducted August 25, 2010.

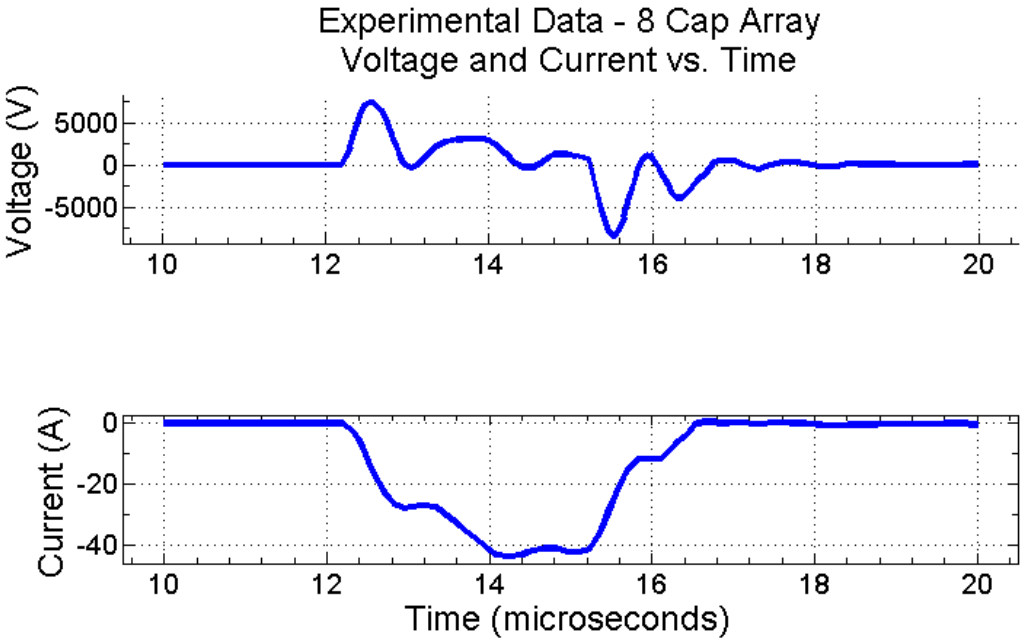

Figure 10. Test 3 - Experimental data consisting of an FEG fired into a circuit with an 8-blasting cap inductance load of 52.2 μH, resistance load of 15.8 ohms and no internal capacitor. Test 3 conducted August 25, 2010.

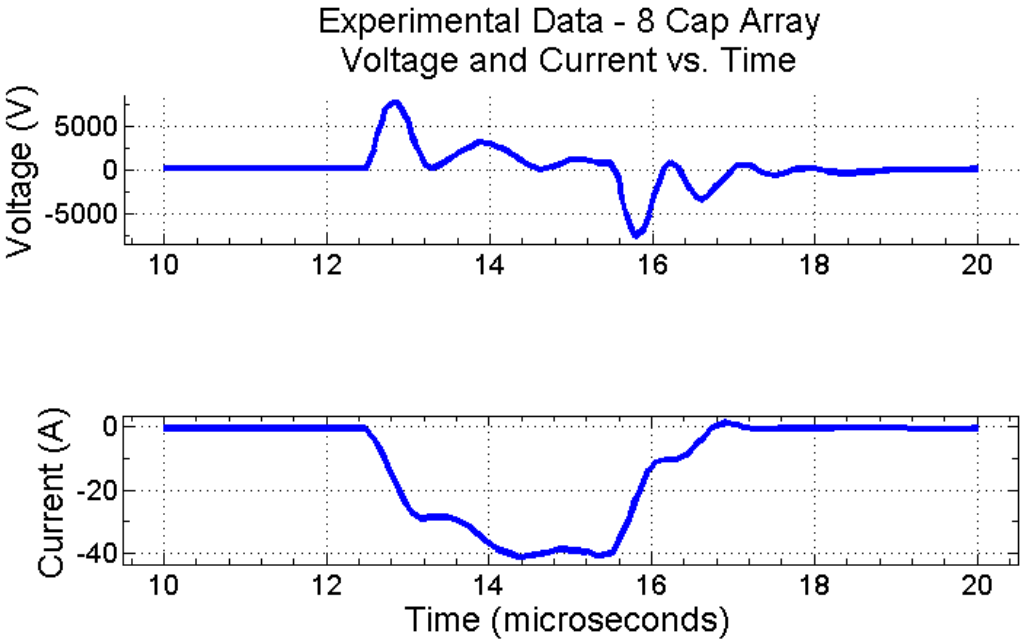

Figure 11. Test 4 - Experimental data consisting of an FEG fired into a circuit with an 8-blasting cap inductance load of 51.6 μH, resistance load of 15.9 ohms and no internal capacitor. Test 4 conducted August 25, 2010.

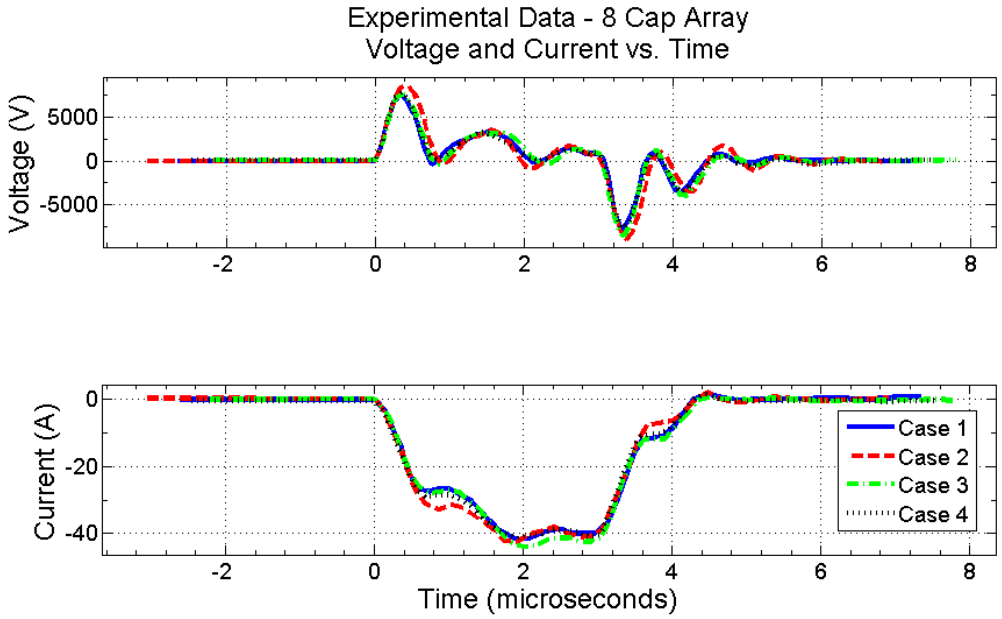

Figure 12. Experimental data showing all four 8-blasting cap load tests with coincident time axis.

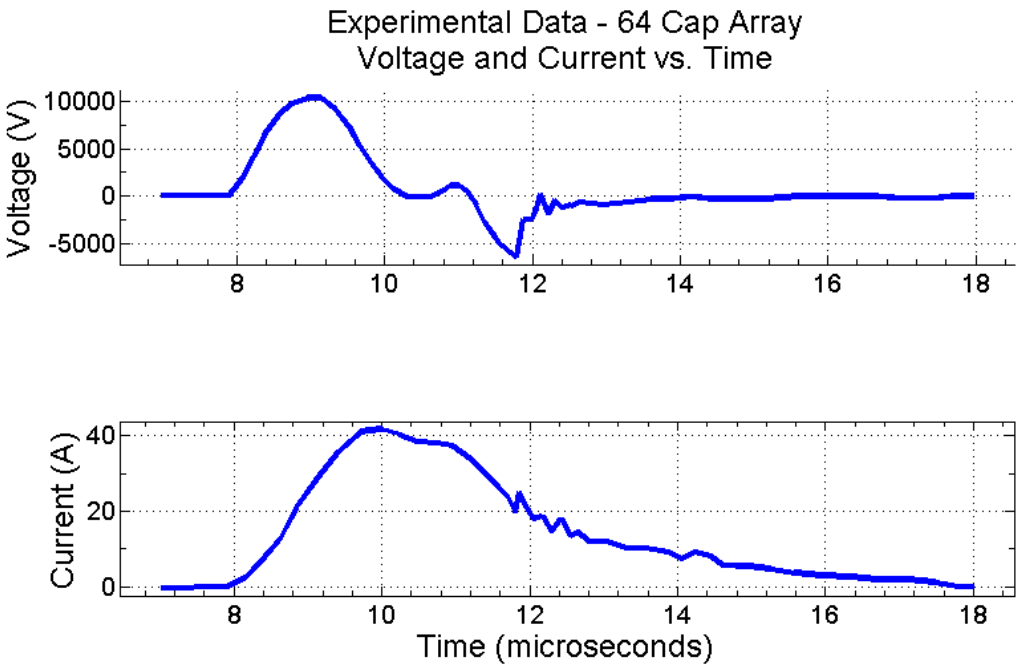

Figure 13. Test 1 - Experimental data consisting of an FEG fired into a circuit with a 64-blasting cap inductance load of 348.8 μH, resistance load of 115 ohms and no internal capacitor. Test 1 conducted March 7, 2011. 49 of 64 blasting caps detonated.

positive while the 8-cap array tests were negative, which is as discussed previously, just a matter of orientation of the PZT, and the data will be kept as provided in the experimental data for comparison to future simulation results. As noted below each of the tests in the corresponding figures, not all of the blasting caps detonated as a result of firing the FEG.

Looking at the experimental data for the 64-cap tests plotted together with coincident time scales provides the same type of information found from the 8-cap data (Figure 16). It is clear that Test 1 and Test 2 of the three experiments share similar graph shapes for both the voltage and current up to the point of the sharp change in voltage and current data in Test 1 that occurs around the 12-μs point in Figure 13 and the 4-μs point in Figure 16 is likely due to either a breakdown occuring in the PZT material before the total release of charge or a measurement device error. There is a difference in the peak values of the voltage for all three of the tests, ranging between

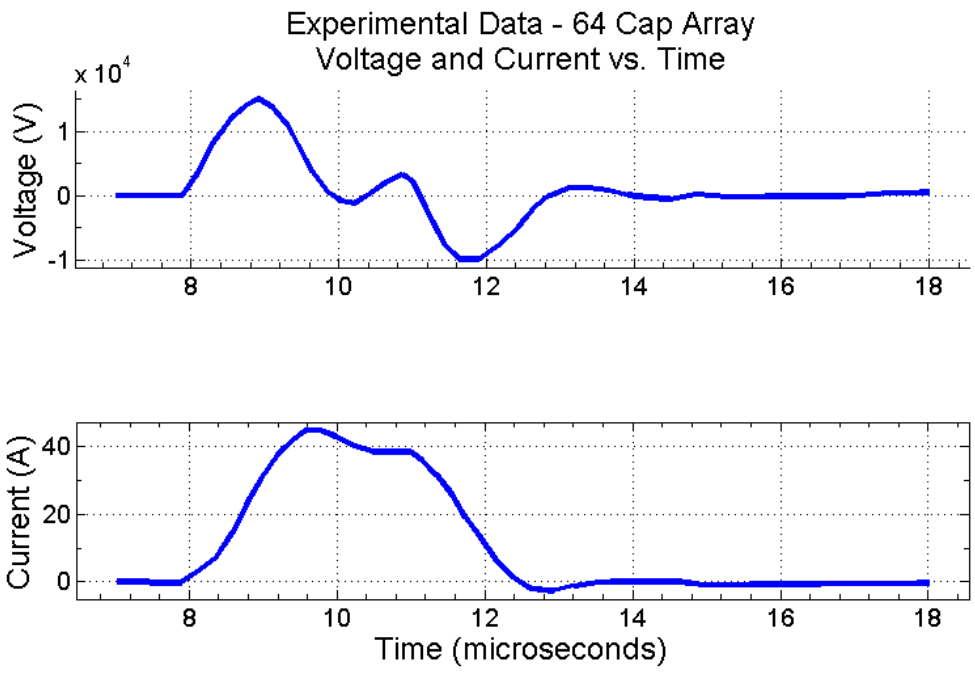

Figure 14. Test 2 - Experimental data consisting of an FEG fired into a circuit with a 64-blasting cap inductance load of 337.8 μH, resistance load of 115 ohms and no internal capacitor. Test 2 conducted March 7, 2011. 47 of 64 blasting caps detonated.

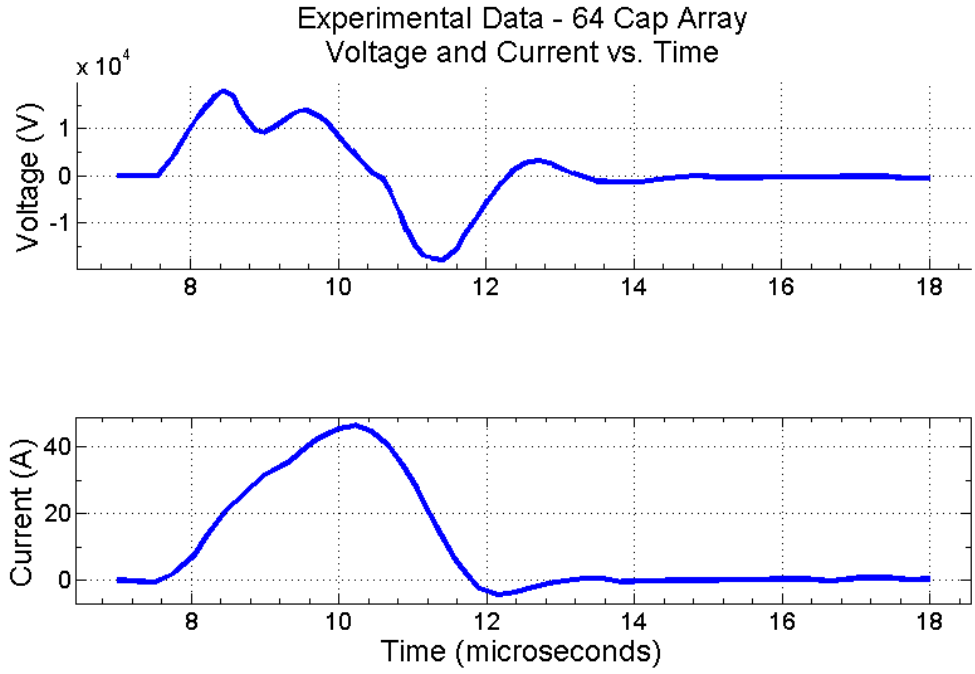

Figure 15. Test 3 - Experimental data consisting of an FEG fired into a circuit with a 64-blasting cap inductance load of 354.9 μH, resistance load of 126 ohms and no internal capacitor. Test 3 conducted March 9, 2011. 63 of 64 blasting caps detonated.

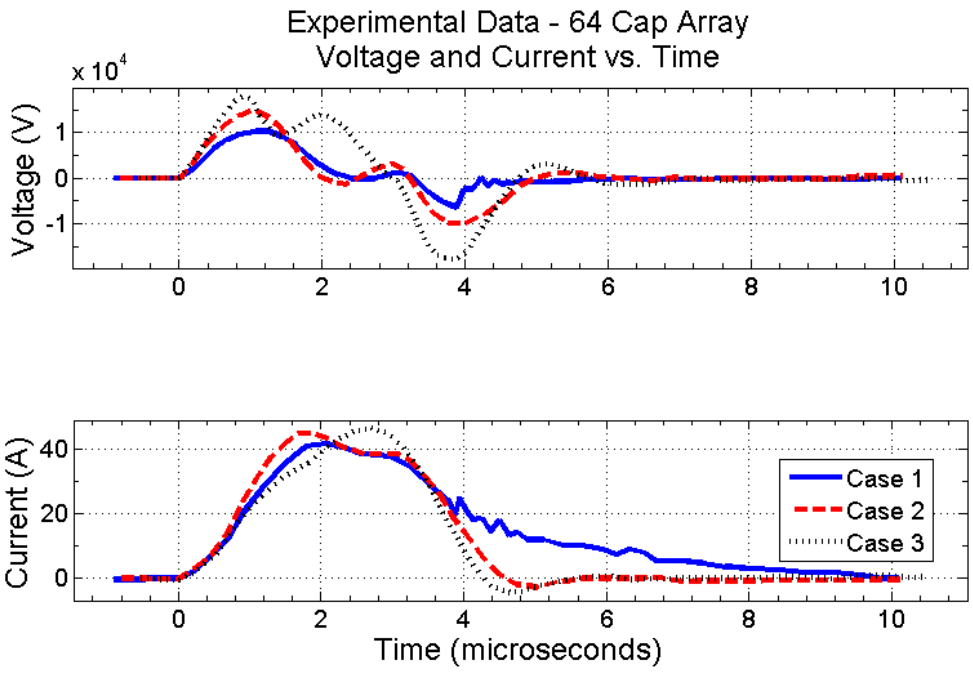

Figure 16. Experimental data showing all three 64-blasting cap tests with coincident time axis.

10,000 volts and just above 18,000 volts. While the shape of the current plots are not the same for the three cases, the peak values are around the same, approximately between 41 and 47 amps.

Noting that for the 64-cap tests all of the blasting caps did not detonate as mentioned earlier, the lack of almost identical experimental results between all three tests (as seen in the 8-blasting cap tests) could potentially be due to any slight changes in the circuit that damaged or defective blasting caps could cause. The differences could also be due to slight variations in the PZT that can occur in production or perhaps due to experimental condition changes. All four of the 8-blasting cap tests were conducted on the same day and therefore likely had the same experimental conditions. The first two cases in the 64-blasting cap tests were also conducted on the same day, while Test 3 was conducted several days later possibly introducing a change in the system that could account for a change in the shape of the graph that is different

than seen in the first two cases.

Considering now the current data for both the 8 and 64-blasting cap scenarios (and ignoring the sign difference), it can be seen that while the shape of the plots is slightly different, the peak value is around the same for each of the tests, approximately between 41 and 46 amps. A similar peak value suggests that while the voltage output from the FEG will vary depending on the circuit load that it is paired with, for this formulation of PZT, the current should be approximately the same in its peak value, though the shape will change slightly with the varying load. Thus, current was considered the most important parameter to be matched throughout the research done here, as modeling the PZT accurately is of primary concern, with voltage matching being of secondary concern.

Circuit Loading

As mentioned above, the test arrays were composed of varied numbers of blasting caps as the electrical load on the circuit. Blasting caps are normally referenced as a resistive element with approximately 2 Ohms of resistance per cap. However, the measured circuit loading for the experiments conducted at Redstone also captured a large inductive loading element. A preliminary part of this research will be to incorporate those measured values along with circuit theory to determine the circuit elements and connections that would best represent the blasting cap load arrays that were tested with the goal of modeling them in ALEGRA.

2.5 Computer Simulation Code Overview

The ALEGRA code is a hydrodynamic finite element code that has been under development by Sandia National Laboratories since the 1990's. It utilizes Arbitrary Lagrangain-Eularian (ALE) modeling to simulate physical deformations, solid dynam-

ics and strong shock physics in two and three dimensions. The ALEGRA family has several variations that incorporate different expansion physics models along with the base ALEGRA modeling capability. The ALEGRA-EMMA code has the ability to model electromechanics and electric circuits coupled with the strong shock modeling and solid dynamics from the ALEGRA basic code, making this code variation a very good choice to use for simulations. The EMMA variant requires a three dimensional mesh. Several of the other variations of the base code include ALEGRA-MHD, which contains physics models for magnetohydrodynamics, and ALEGRA-HEDP, which builds on the ALEGRA-MHD version and adds physics model that allow simulation of high energy density applications.

Arbitrary Lagrangian-Eularian

Because ALEGRA was designed as a code to be used to simulate strong shock physics and large deformations, the use of simple Eulerian methods of finite element formulation where the mesh and coordinate frame are fixed in space is not always suitable since material boundaries can cause issues and decrease accuracy. Lagrangian finite element codes, where the reference frames are attached to the material itself, are also not always suitable since large material deformations can cause mesh distortions that result in simulation convergence failure. With large velocities and density and pressure gradients that can be caused by strong shock physics, a hybrid scheme is sometimes required in order to deal with potential problems that can arise in each type of simulation.

The hybrid scheme is called Arbitrary Lagrangian-Eularian. An ALE method combines the best attributes of both traditional finite element methods. The method includes a mesh that moves as time progresses, but is still independent of the actual material motion, thus allowing the simulation to adequately handle material bound-

aries while still maintaining good accuracy. The downside of the ALE formulation is that computational implementation requires a more complex update procedure for the mesh at each time step that strongly affects the success of the simulation. The specifics of the ALE formulation of kinematics can be found in Chapter 14, Volume 1 of the "Encyclopedia of Computational Mechanics" (7). The chapter also discusses the difference in the formulation of the governing conservation equations for the ALE finite element scheme which now require the addition of the mesh and material relative velocities, called the convective velocity.

The benefit of ALEGRA as an ALE code is that it allows the user to specify the needs required to simulate a specific problem, which can include areas of a mesh that are Eulerian in nature and areas that are Lagrangian in nature as well as areas that employ the hybrid ALE scheme. The ability to choose the finite element method is especially useful with a multi-material system with boundaries and interfaces that have different constraints than elements in the middle of a material mesh and are subjected to very strong mechanical and electrical forces.

Operating Methodology

The basic governing conservation equations and operating methodology of the ALEGRA code are summarized in the paper titled "ALEGRA: An Arbitrary Lagrangian-Eulerian Multimaterial, Multiphysics Code" (9). The code involves equations that deal with radiation-magnetohydrodynamics. The EMMA version also includes governing equations that deal with electromechanics and circuits. The governing equations are applied first in a Lagrangian step where the mesh is moved with a calculated velocity based on stresses in the system.

In the next step, called the remesh step, the code utilizes several mesh enhancement algorithms to smooth out and optimize the mesh that was moved in the previous

Lagrangian step. The remesh attempts to prevent distortions in the overall mesh that would otherwise create inaccuracies in the nodal and element parameter calculations. It also defines a relative velocity of the mesh for use in the next step.

The third step in the process is called the remap step. In this step, the relative velocity that was calculated in the remesh step is taken, and the variable parameters that were calculated using the governing equations are projected onto the new mesh.

One of the issues with using ALE codes lies in the fact that they inherently have problems with energy conservation. For ALEGRA, the concern about energy conservation arises in the remap step where the kinetic energy must be calculated and projected to the new mesh. The code uses internal energy in the calculations rather than total energy. The code does include an algorithm that will partially correct the energy drift that occurs upon remapping, known as the DeBar fix (9), which is the default procedure that ALEGRA will follow unless the user specifies otherwise. ALEGRA does have an option that can be called by the user in the input file that will conserve total energy, but doing so can cause instabilities in the code solutions (3). For the most part, the non-conservative energy issue is seen as system temperature differences between the simulation data and what would be expected in a real system. For most simulated systems this temperature difference does not pose a significant problem and the more stable non-conservative algorithm can be used without affecting the simulation output overly much.

Materials

The ALEGRA code includes a wide variety of materials in a material library that the code uses to specify and call mechanical and electrical properties that will be used in the calculations. A base model for a ferroelectric ceramic material was developed and is included in the material library for the EMMA version. However, since the

funding for this area of research was cut, the model was not fully developed and much work was needed to make the model operational. The code also allows for user definition of material properties if needed for specification of a problem, which is very important as it gives the flexibility to optimize the ferroelectric material model to meet experimental needs as will be done in the course of this research.

Breakdown Modeling

As was mentioned in the section above discussing dielectric material breakdown, the phenomenon itself is a very complex issue. The breakdown that occurs spans across multiple physical mechanisms. Being able to model them accurately would require a code that incorporated all of the physical models and executed them simultaneously. Currently, the ALEGRA-EMMA model does not have the capability to simulate breakdown. Successful simulation would require that the ALEGRA-EMMA and ALEGRA-MHD codes operated together and were able to pass information between each and transition solutions in order to achieve an accurate representation of the phenomena. There is no current plan on the part of Sandia National Laboratory to pursue this modeling capability.

Additional Software

Another software program that was used in researching this problem was CUBIT (10), also developed by Sandia National Laboratories. CUBIT is a three-dimensional computer aided design program that is external to the ALEGRA code that can be used to build the 3D computer model and mesh a grid for more complicated shapes and designs. It allows for the use of different computational grids and meshes for different areas of a problem to capture all of the important physical deformations of the problem.

III. Methodology

3.1 Chapter Overview

Chapter 3 will discuss how the FEG model was compiled and simulated. The first two sections focus on the the physical model of the FEG, to include the block of PZT material and how these are represented in the ALEGRA code. The third section describes the specifics of modeling the circuit load that the FEG was attached to for the experimental tests. The next section includes the three scenario studies that were done in the course of this research. The last section discusses the data analysis techniques that were used for the ALEGRA-EMMA data output and the data visualization methods that were used to effectively present the case study data.

3.2 Modeling the FEG

Researching this problem was broken down into three different (but interrelated) steps. Modeling the specific FEG design was the first part of the problem. The computational model of the Redstone designed FEG was compiled using the engineering schematic drawings (see Appendix A) that were provided by the US Army. The design was computationally constructed and meshed using the CUBIT software meshing program. The C-4 explosive was modeled using the ALEGRA library values for the yield, detonation and property models. The potting material and housing case were represented by polymethyl methacrylate or PMMA, a synthetic polymer plastic that is also known commercially as Plexiglas or Lucite. This material was chosen for its full property model availability in the ALEGRA material library and the fact that the material properties allow it to not participate in or affect the electrical circuit portion of the simulation.

Initially a coarse mesh of 10 elements per centimeter was chosen for simulation

to reduce computational time. These results were compared with several finer mesh grids which took a much greater computational time. The finer grids tested were at 50 elements per centimeter and 100 elements per centimeter. Initial example results indicated that a finer mesh did not change the response curves for voltage and current, so all subsequent simulations were performed with the coarser mesh, allowing for more simulation runs to be achieved. The final mesh dimensions chosen were 10 elements per centimeter of the model object.

Included in the model is a metal plate at the very bottom of the grid. The plate was not part of the experimental setup in any way. It is only included in the model as a means to contain the explosive products that are created as a result of detonation. Without the plate, the gases expand beyond the grid faster than the shock wave propagation through the PZT material and cause instabilities in the element calculations for the code that cause it to fail and a much larger grid area would be required in order to obtain the same simulation time. Expanding the grid to accomodate the detonation products without the metal plate results in a simulation that takes much longer to converge on a solution. The inclusion of the plate does not affect the modeling of the FEG output in any way other than to allow a longer simulation time as there are no reflected waves that will interfere with the PZT block.

3.3 Modeling the PZT

Modeling the PZT accurately was the next part of the problem. The PZT model parameters are a large part of what determines the values of the current and the voltage in the simulation response. Incorrect values in the model would prevent achieving a match between experiment and simulation. Some of the parameter values were determined from known information about the specific PZT formulation used in the experiments that was provided by TRS technologies as well as from information

collected and presented in the Setchell papers (12; 13). With this in mind, a study of the PZT parameters that most affected the simulations outcome was performed. Background research and some preliminary test simulations suggested that density, remnant polarization, saturation, phase transition rates and permittivities were very important to the response.

A baseline simulation was performed using the open circuit loading with the PZT parameters provided by SNL in the PZT library model. Additional simulations were then performed to incorporate changing the variable parameters of the Redstone PZT in order to see what effect they had on the shape of the open circuit curve by comparing it to the baseline SNL model simulation and to see what effect they had on the shape of the curves as compared to the 8-blasting cap and 64-blasting cap experimental cases.

From the information provided by TRS technologies, the density of the material was determined to be 7.9 grams per cubic centimeter. This parameter then did not need to be varied through the simulations.

The second variable parameter examined was the saturation, the ratio of remnant polarization to spontaneous polarization. Data of the polarization vs. electric field strength of the TRS PZT 95/5 formulations showed this parameter ranging between 0.75 and 0.95.

The next parameter was the remnant polarization value. This value is the macroscopic polarization in coloumbs per square meter. For the TRS PZT formulations, this value ranges between 0.27 to 0.38 Coloumbs per square meter.

Another set of parameters that was studied were the permittivities of the ferroelectric and antiferroelectric states. Previous research (13) suggested that the values for both parameters would be on the order of 1×10^{-9} to 1×10^{-8} Farads per meter. A value for the permittivity of the ferroelectric state was found in the TRS PZT

data. This value correlated well with the assumed order from previous research, with a value of 2.61×10^{-9} Farads per meter. The values for the permittivity of the anti-ferroelectric states are almost impossible to measure and must be estimated, which gave the ability to vary this value more widely and allow for a better optimization type process to occur when determining the final value of this parameter.

3.4 Modeling the Circuit Load

Modeling the circuit load for each case was the third and final aspect of being able to correlate the simulation results against the experimental results. The three scenarios chosen were an open circuit load, an 8-blasting cap load and a 64-blasting cap load. As discussed in Chapter 2, these were chosen based on the availability of range measurement data of the inductance and resistance values of the assumed circuit. The open circuit case was the easier case to model from the circuit load perspective as there were no circuit elements to be included in the model. The open circuit scenario and its four test cases are described below in the Open Circuit subsection of the Test Cases section.

Modeling the cases that included blasting caps (i.e., a circuit load) required a more in-depth look at circuit theory. The experimental setup for each test completed at Redstone measured an inductance and a resistance value for each blasting cap load array with an assumed circuit of an ideal resistor in series with an ideal inductor. These values were measured using a commercially available LCR meter. As a standard, blasting caps are referenced as a resistance load at approximately 2 Ohms per cap. For this setup, the extra wiring and the way the array was manufactured created an inductance loading as well that outweighs the simple resistance loading factor and so must be included in the model. A small capacitance of 9 picoFarads also existed in the circuit due to the presence of the voltmeter. While the assumed circuit setup was

likely the correct assumption for the circuit loading to use in the simulation, in order to thoroughly investigate this problem, several other circuit loading combinations were also considered.

There were five total circuit loading combinations that were considered. The first three models used lumped circuit element modeling techniques. The three lumped element circuit loads that were considered for this problem were: an ideal resistor in series with an ideal inductor (Circuit 1) also known as a simple non-ideal inductor model, a small-valued ideal capacitor in parallel with an ideal resistor in series with an ideal inductor (Circuit 2) also known as a more complex non-ideal inductor model, and an ideal inductor in parallel with an ideal resistor (Circuit 3) another form of the simple non-ideal inductor model. The last two circuit models did not use the lumped element loading. The first model was pairs of ideal resistors in series with ideal inductors, where the pairs were then in series (Circuit 4) essentially trying to model each blasting cap as a non-ideal inductor as in Circuit 1. The last circuit was modeling the load as pairs of ideal resistors in parallel with ideal inductors, where the pairs are then in series (Circuit 5) essentially modeling each blasting cap as a non-ideal inductor of the type in Circuit 3. Figure 17 shows a graphical depiction of these five circuit models.

To model the circuit elements in ALEGRA-EMMA, the input deck needs to specify element nodes and the circuit element and corresponding value that connect each node. It was quickly realized upon early simulation that the differential equation solver that is used in the EMMA simulations was not readily equipped to handle large amounts of element nodes. The simulations failed relatively early in the calculations due to the large amount of nodes that would need to be specified to simulate circuits 4 and 5. Thus, those circuits were eliminated from the comparison and it was determined that a lumped circuit element model was required.

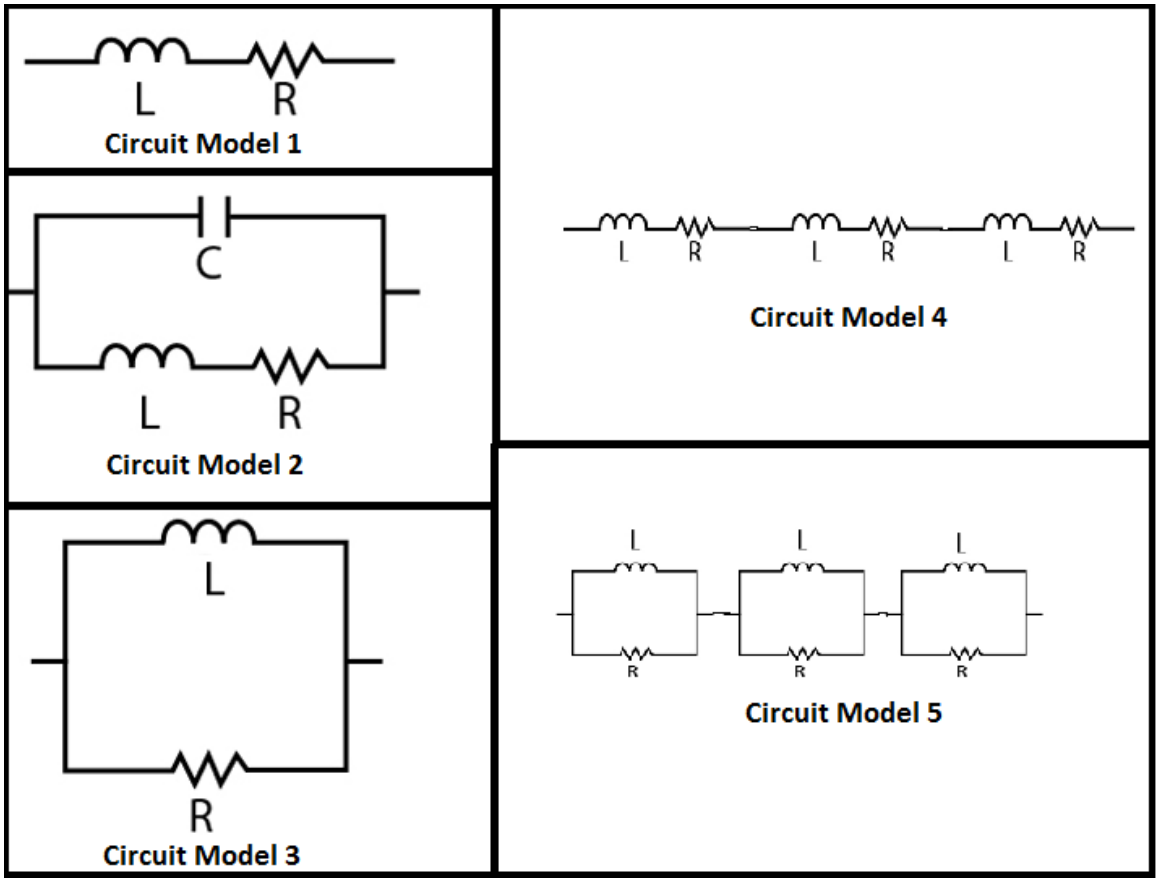

Figure 17. The five circuit models considered for use in the simulation of Redstone FEG experimental setup. L represents the inductance value, R represents the resistance value, and C represents the capacitance value

3.5 Test Cases and Analysis Techniques

Scenario 1: Open Circuit

For the open circuit model, as stated above there were no circuit elements included. The circuit then consisted of the PZT block with nodes attached to the upper and lower faces of the block with node 1 being set to ground. The voltage in the code is then measured at node 2 to determine the voltage difference between node 1 and node 2. The voltage output from this case allowed a comparison between simulation and experimental data to occur in order to study the effects of varying PZT model parameters on which the results were thought to be dependant.

Once the final PZT model was determined, the open circuit case was run to be compared against the data collected for the four open circuit test cases discussed in Chapter 2. Only one simulation was run to use as a comparison.

Since, as discussed in Chapter 2, all of the open circuit experimental test results end with breakdown of the PZT material, the peak values seen in the test curves only represents at what point breakdown occured and provided no actual values that could be used to measure the simulation results against. The ALEGRA-EMMA model does not currently model breakdown, either mechanical or electrical. Therefore, the only comparative capability and analysis available was to be able to match the slope of the voltage curve between the experimental and the simulation data for the amount of time that experimental data was collected. A matching slope would give indication that the PZT in the model was behaving as the PZT in the experiments.

Scenario 2: 8 Blasting Cap Load

Once the final circuit loading and PZT models were determined, the four cases that were discussed in Chapter 2 were simulated in ALEGRA-EMMA. These four simulation cases are listed below in table 4.

Table 4. 8-Blasting Cap Array Test Cases.

Run Number	**Inductance** μH	**Resistance** Ω
8 Cap-Case 1	42.9	15.9
8 Cap-Case 2	58.6	16.0
8 Cap-Case 3	52.2	15.8
8 Cap-Case 4	51.6	15.9

The voltage and current time histories that were generated by the ALEGRA code were taken and visually compared to the experimental data curves by overlapping the data in graphical form. Peak values of current and voltage as well as their respective rise times were also found as a comparison to the experimental data.

Scenario 3: 64 Blasting Cap Load

Once the final circuit loading and PZT models were determined, the three cases that were discussed in Chapter 2 for the 64-blasting cap arrays were simulated in ALEGRA-EMMA. These three simulation cases are listed below in table 5.

Table 5. 64-Blasting Cap Array Test Cases.

Run Number	**Inductance** μH	**Resistance** Ω
64 Cap-Case 1	348.8	115
64 Cap-Case 2	337.8	115
64 Cap-Case 3	354.9	126

The voltage and current time histories that were generated by the ALEGRA code were taken and visually compared to the experimental data curves by overlapping the data in graphical form. Peak values of current and voltage as well as their respective rise times were also found as a comparison to the experimental data.

3.6 Data Visualization and Analysis Tools

One of the basic tools of analysis and visualization that will be used is Paraview (2), a data analysis package that allows three dimensional simulation playback while viewing any of the output parameters of the ALEGRA-EMMA code. Paraview allows the user to view the time history of a particular parameter in a three dimensional space to verify that the progression is as expected. It also gives the user the ability to view the distortion and deformation that is occuring as the simulation progresses.

Another tool that can be used as part of the ALEGRA suite of codes is a plotting program called Hisplot, which is a simple line-plotting tool that can generate graphs of the time histories of global variables. The program is a useful way to quickly verify and visually compare the general shape of the voltage and current simulation data against the known experimental data while the simulation is running and to easily compare the differences that are produced when varying input material parameters.

In addition to the two programs above that are commercially available, MATLAB® was used to develop several analysis scripts specifically for this problem that were used to calculate and extract information from the simulation data, such as rise times and peak values. Scripts were also written to graphically compare the simulation plots of voltage and current against the experimental data in each test case in the test matrix.

MATLAB® was also used to write several scripts that used circuit differential equations and the digitized experimental data curves for the current to predict the voltage output curves. Scripts were written to represent the different options of circuit load representation discussed above and used to compare against the given digitized voltage data for each of the two blasting cap load scenarios in order to best estimate what circuit load produced the correct voltage curve shapes.

IV. Results and Analysis

4.1 Chapter Overview

The objective of this research was to determine the feasibility of creating a computer model to validate the experimental results that were recorded from tests conducted by the US Army at Redstone. The first two sections describe the analysis and selection of the final PZT and circuit loading models that were chosen to perform the scenario simulations. The last three sections show the results from the open circuit, 8-blasting cap load and 64-blasting cap load cases and compares the simulation results to the experimental data that was previously collected.

4.2 PZT Model

Finalizing the PZT model required many simulations and comparing the output data to the experimental data. The intent was to find the combination of the computational PZT parameters that allowed the solution to most closely match the experimental data while still being within an acceptable range of values for each parameter. The five parameters that were studied were the phase transformation rate, the permittivity of the ferroelectric state, the permittivity of the antiferroelectric state, the saturation, and the remnant polarization. The final parameter values that were chosen to best represent the PZT material that was used in the experiments conducted at Redstone are shown in Table 6. All other parameters were kept the same as the model developed initially at SNL.

The relationship between the material parameters and their effect on the simulation output is very complex and interrelated. The coupled nature of the parameters made the process of determining the final values more complicated. Instead of determining each value individually, the trends that were produced from varying each

Table 6. Final values chosen for the PZT model.

Parameter	**Value**	**Units**
FE permittivity	2.61×10^{-9}	$Farads/meter^2$
AFE permittivity	1.99×10^{-8}	$Farads/meter^2$
Phase transition rate	300	μs^{-1}
Saturation	0.75	*none*
Remnant polarization	0.29	$Coloumbs/meter^2$

parameter were examined and used to select the final set of parameter values.

The values picked for the saturation and remnant polarization are both within the expected range of values that were previously determined from background research. From simulation trials it can be seen that the saturation and the remnant polarization parameter values affect the peak values of the voltage and the current curves. The parameter values were varied until the current peak value was within the range of values seen in the experimental data for both the 8-blasting cap and 64-blasting cap cases. It will be shown later that while it is possible to match the current with the final choice of parameters, the voltage values do not match for either case. Possible explanations will be discussed in the sections that show the simulation data.

It can also be seen from simulations that the permittivity of the ferroelectric state and the permittivity of the antiferroelectric state do not have as much of an impact as the ratio of the permittivities. The permittivities when varied individually only slightly change the shape of the voltage and current curves, particularly with respect to the ratio of local peak heights. The ratio of the permittivities however affects the shape of the curves with respect to how quickly the material reacts and the time scale of the reaction as well as the ratio of the peak heights. The combination of both the individual values and the ratio of permittivities were used to select parameter values that produced simulation output with a shape similar to the experimental data for the current and voltage in both the 8-blasting cap and 64-blasting cap cases. While the

permittivity of the ferroelectric state was eventually chosen to be the value provided by the TRS material information sheet, the permittivity of the antiferroelectric state is much higher. It was discussed in Chapter 2 that the antiferroelectric permittivity is typically an estimated value and it is typically a slightly smaller value than the ferroelectric permittivity. Looking at the final value used for the model, it is clear that the value is much larger than the ferroelectric permittivity. Even though it is much higher than expected the value still provides an acceptable solution possibly due to the fact that, as discussed, ALEGRA-EMMA does not include a breakdown model and having a larger permittivity in the antiferroelectric state could in part make up for that fact, as a larger permittivity means a higher capacitance and lower voltage output, thus simulating the results of breakdown.

Varying the phase transformation rate through the simulation trials doesn't have a large effect on the overall simulation output, but it does produce slight changes in the behavior of the curves around the local peak values, especially for the current curves, and also affects the ratio of the local peak heights. Since there was no actual range of values that was determined from the background literature, the final value was chosen as the value that produced simulation curves that best matched the experimental results.

4.3 Circuit Loading Model

As discussed in Chapter 3, only the lumped circuit element models were considered after initial examination of test simulations. These were the first three circuits described, all variations of the non-ideal inductor model. The three models were used in a MATLAB® script (Appendix B) that used the differential equations of the model to propagate a voltage output from the digitized experimental current data. The current was used since the magnitude of the current was approximately the same

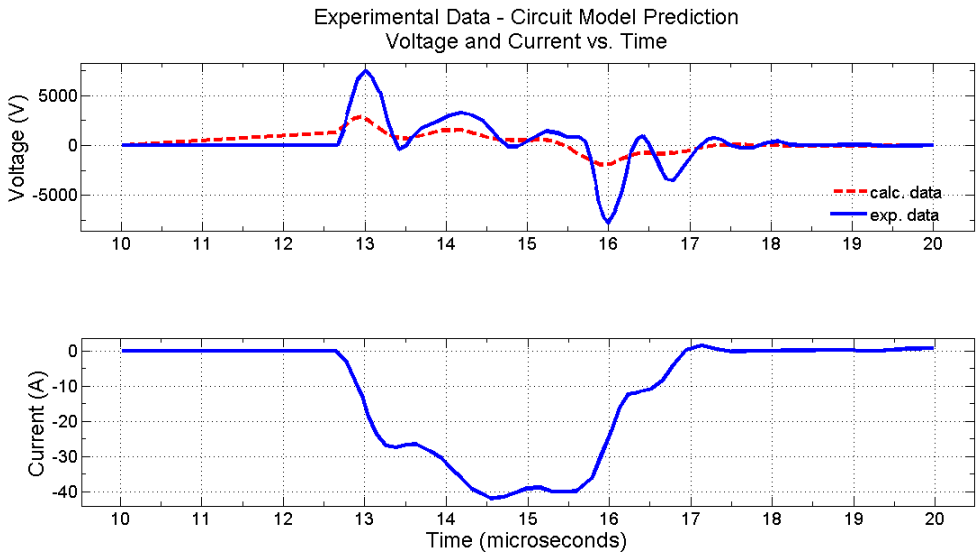

Figure 18. Circuit Model 1: 8 cap - Plot showing comparison of Circuit Model 1 to experimental data for the 8-blasting cap scenario.

between both the 8-cap and 64-cap experimental tests. The voltage prediction was compared to the digitized experimental voltage data to see if the pattern could be reproduced. The three circuit model comparisons are shown for the 8-blasting cap case in Figure 18 to Figure 20 and 64-blasting cap case in Figure 21 to Figure 23.

From Figures 18 and 19, it can be seen that the differential equations provide a similar voltage response curve to the same input current for the 8-blasting cap case, which is to be expected since the circuit models are similar except for the small-valued capacitor that exists in Circuit Model 2. Both circuit models also show a response pattern that is in line with the experimental pattern seen in the voltage, as far as where peak values are located. The actual values for the voltage do not match the experimental data, but that is to be expected as this is a dynamic system where feedback between the FEG and circuit load can occur which may not be able to be captured by the simple circuit differential equation models. Similar results are seen when comparing Circuit Model 1 and 2 for the 64-blasting cap case in Figures 21 and 22, though in these model comparisons there is a better match to the peak voltage

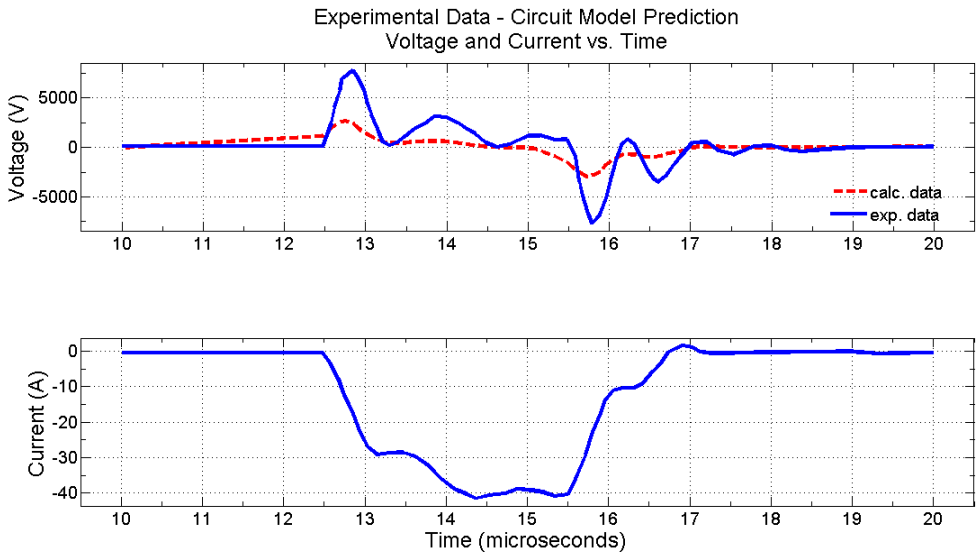

Figure 19. Circuit Model 2: 8 cap - Plot showing comparison of Circuit Model 2 to experimental data for the 8-blasting cap scenario.

values.

From Figure 20 it can be seen that Circuit Model 3 does not produce a voltage output that matches the pattern of the experimental data for the 8-blasting cap case. The same result is also seen in Figure 23 for the 64-blasting cap case. The pattern of the peak value occurances is not consistent with collected data. From these two figures, it can be determined that this is not an acurate model to use to represent the circuit loading in the experimental setup.

The analysis so far left Circuit Model 1 and 2 as viable circuit loading models to use for the simulations. Both models were run in the ALEGRA-EMMA environment and the final circuit was chosen based on which model produced a better response curve in comparison to the experimental data for the current.

From sample comparisons it was seen that Circuit 1 provides a slightly better overall shape, though there is very little difference between the simulation results, which confirms that the initial guessed circuit loading model is the correct model to use and that the small capacitance that exists due to the voltmeter does not need

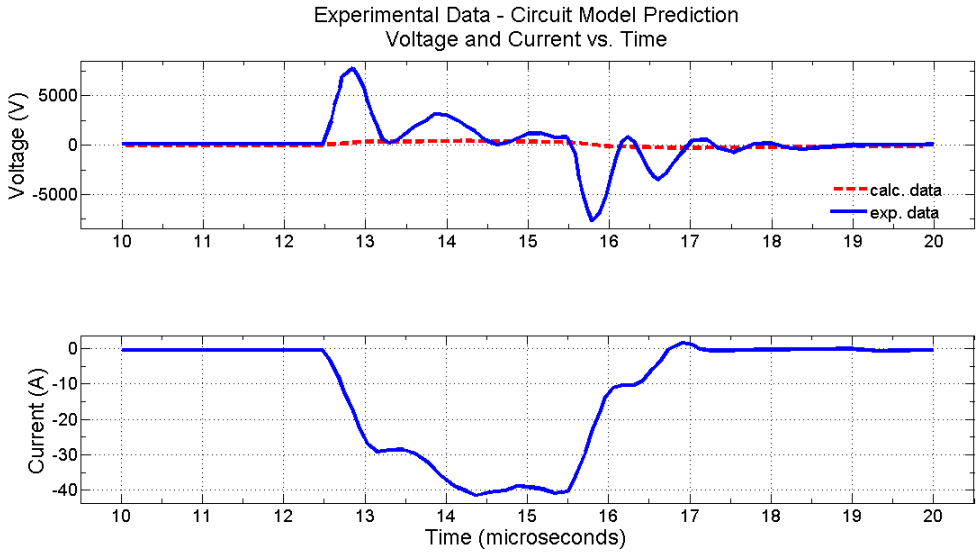

Figure 20. Circuit Model 3: 8 cap - Plot showing comparison of Circuit Model 3 to experimental data for the 8-blasting cap scenario.

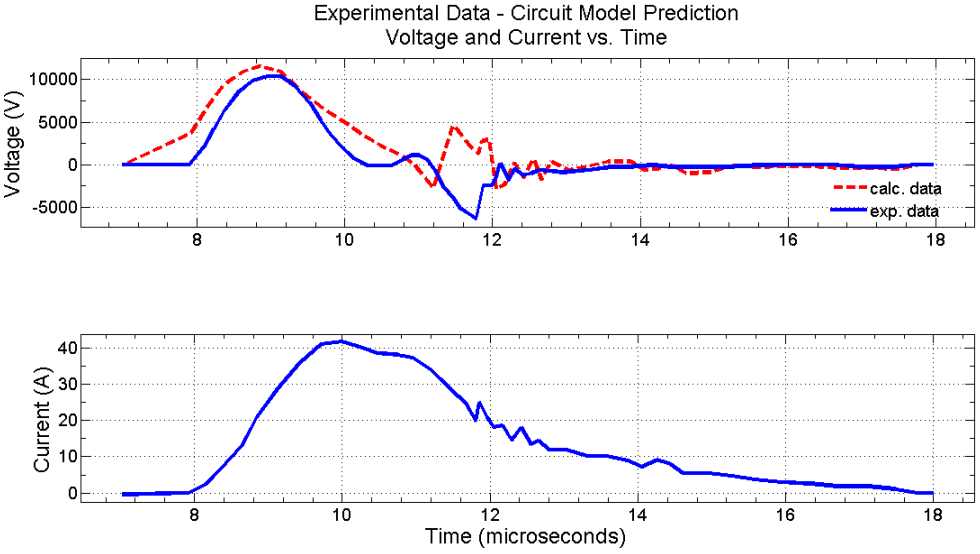

Figure 21. Circuit Model 1: 64 cap - Plot showing comparison of Circuit Model 1 to experimental data for the 64-blasting cap scenario.

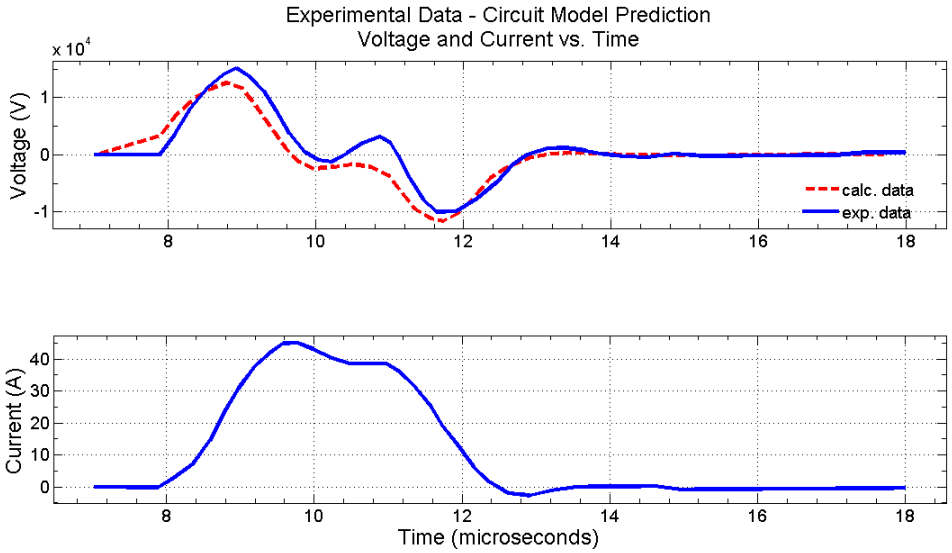

Figure 22. Circuit Model 2: 64 cap - Plot showing comparison of Circuit Model 2 to experimental data for the 64-blasting cap scenario.

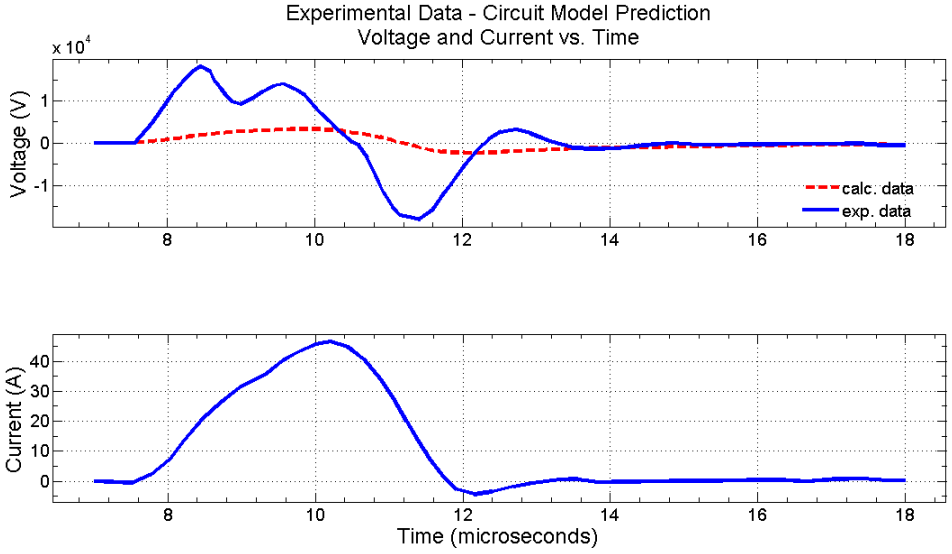

Figure 23. Circuit Model 3: 64 cap - Plot showing comparison of Circuit Model 3 to experimental data for the 64-blasting cap scenario.

to be included in the circuit model. The following analysis for the two experimental scenarios where circuit loading exists is done using Circuit Model 1.

4.4 Scenario 1: Open Circuit

The first scenario that was simulated was the open circuit case. The scenario was only simulated once and compared against each of the four provided experimental open circuit cases. The final FEG simulation design as seen in the visualization software Paraview can be seen in Figure 24, which shows the plotted density in order to distinguish materials. The density in the diagram is measured in kg/m^3.

Figure 25 shows the comparison between the experimental data for Case 1 and the simulation data as created by plotting each against a coincident time scale using MATLAB®. From the top graph in this comparison, it can be clearly seen that the simulation data continues well beyond the peak value where the experimental data shows breakdown, a symptom of the ALEGRA code's inability to model breakdown. The bottom graph in this comparison shows the same data with a "zoomed in" view around the experimental peak and a dashed red line that projects the slope of the experimental data further on the time scale for comparison of the slope between the simulation and experimental data. It was discussed previously that without a valid breakdown model, the only comparison that was available for the open circuit scenario was to compare the slopes of the data. From this view it can be seen that initially at the start of the reaction the simulation data has a similar slope, but eventually the slope of the simulation data increases past that of the experimental data. The unmatched slope could indicate that the reaction speed of the PZT material in the simulation still does not match that of the experimental PZT.

Figures 26 through 28 show the comparison between the experimental data and the simulation data for Cases 2 through 4, respectively. In all of the comparisons for

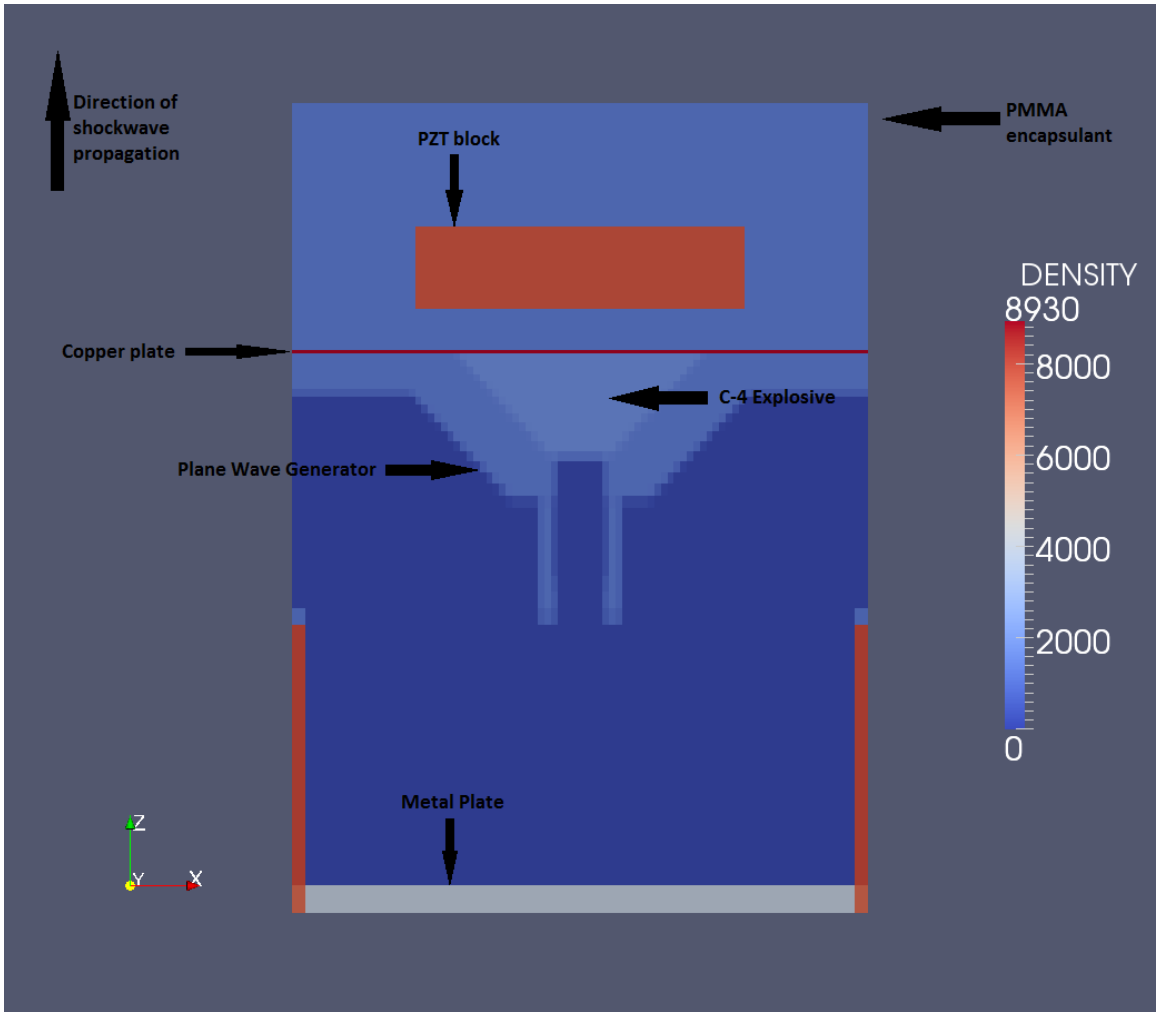

Figure 24. Visualization of final FEG design as seen in Paraview, clipped view through center of FEG. Diagram shows density to show separate materials.

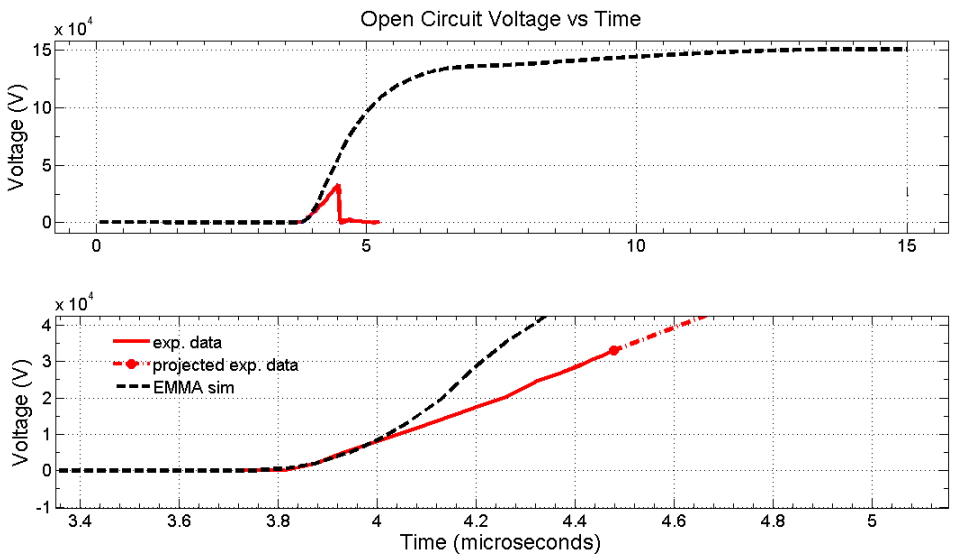

Figure 25. Case 1 - Plot showing comparison of ALEGRA-EMMA simulation to recorded experimental data of open circuit.

the remaining three cases, the graphs show the same results that are seen in Case 1. Even Case 4, where breakdown is suffered at a higher voltage level than the other three cases, shows the same trend as discussed in the Case 1 results.

In addition to the output voltage and current plots, other data can also be seen using Paraview to give a three dimensional view of simulation results and to see if the simulation is proceeding as expected. One of the areas that was examined was the deformation that would be expected from a reaction of this kind. From the experiments, it was seen that the failure of these tests was catastrophic and the assembly tore itself apart during the reaction. In the ALEGRA-EMMA code, there is no fracture and void-insertion model as there is in other versions of the code. Therefore, we would not expect to see the assembly tear itself apart as in the experiment, but do expect deformations to occur. Figure 29 shows the comparison of the density of the materials before the start of the reaction (left) and after the reaction has concluded (right). Clearly, there is deformation that occurs in that the PZT block and copper plate have been curved in the direction of the shockwave propagation and

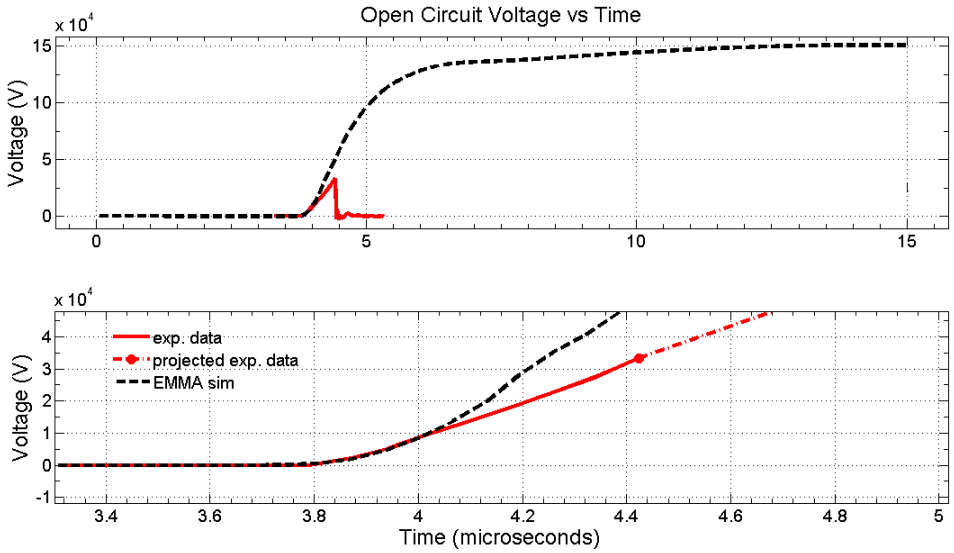

Figure 26. Case 2 - Plot showing comparison of ALEGRA-EMMA simulation to recorded experimental data of open circuit.

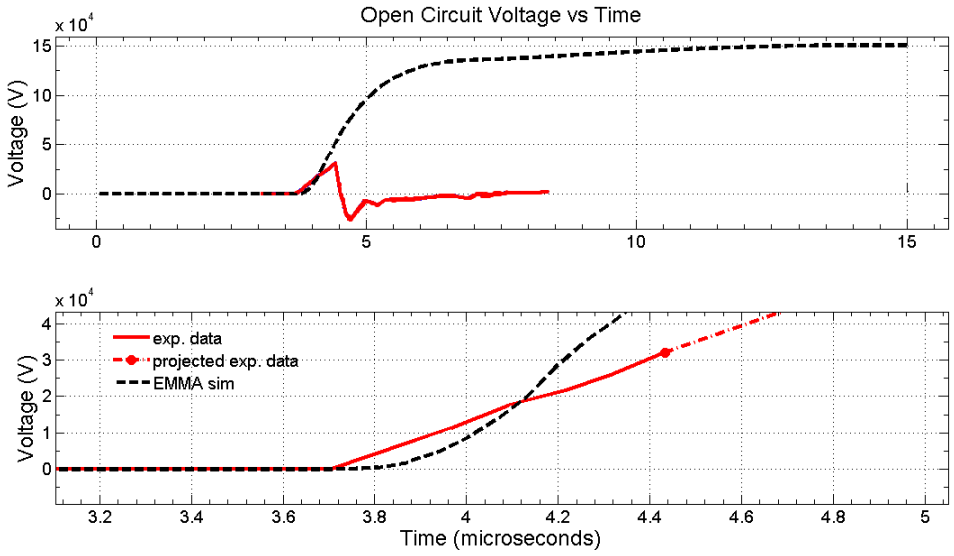

Figure 27. Case 3 - Plot showing comparison of ALEGRA-EMMA simulation to recorded experimental data of open circuit.

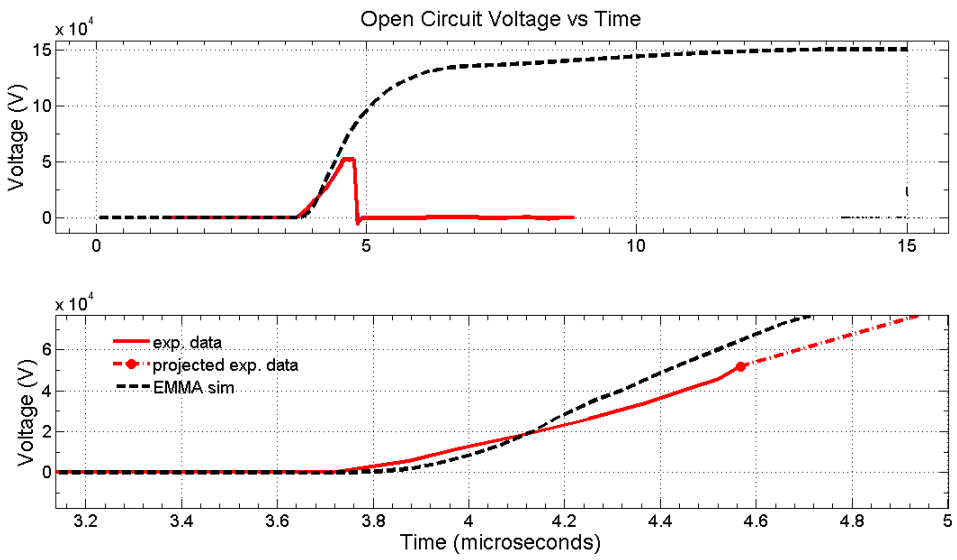

Figure 28. Case 4 - Plot showing comparison of ALEGRA-EMMA simulation to recorded experimental data of open circuit.

the triangular plane wave generator has been expanded outward from the inside cavity that used to contain the C-4 explosive. The density in the diagram is measured in kg/m^3. These are in line with the deformations that would be expected, given that the model can not fracture.

Another check of the simulation is to look at the shockwave propagation. The intent of the Redstone FEG design was to have a planar wavefront as it reaches the copper plate so that the PZT can be uniformly depolarized. Figure 30 shows the shockwave front as it reaches the copper plate. The left picture shows the density, and the different material elements can be distinguished, while the right picture shows the pressure in N/m^2. From these two diagrams it can be seen that the wavefront hits the copper plate with an almost planar front, though still slightly curved. If the wavefront in the experiments is actually planar, then the difference in the wavefront shapes could cause some of the discrepancies that are seen in the simulation comparisons of voltage and current.

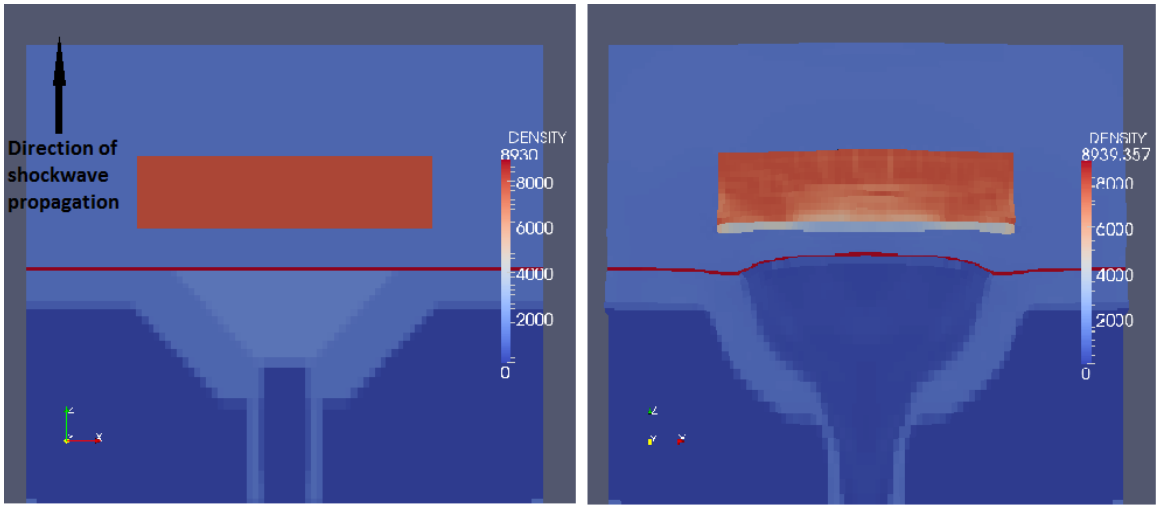

Density - Before

Density - After

Figure 29. Visualization of density in FEG simulation before (left) and after (right) shock wave has passed through, showing deformation that occurs in materials.

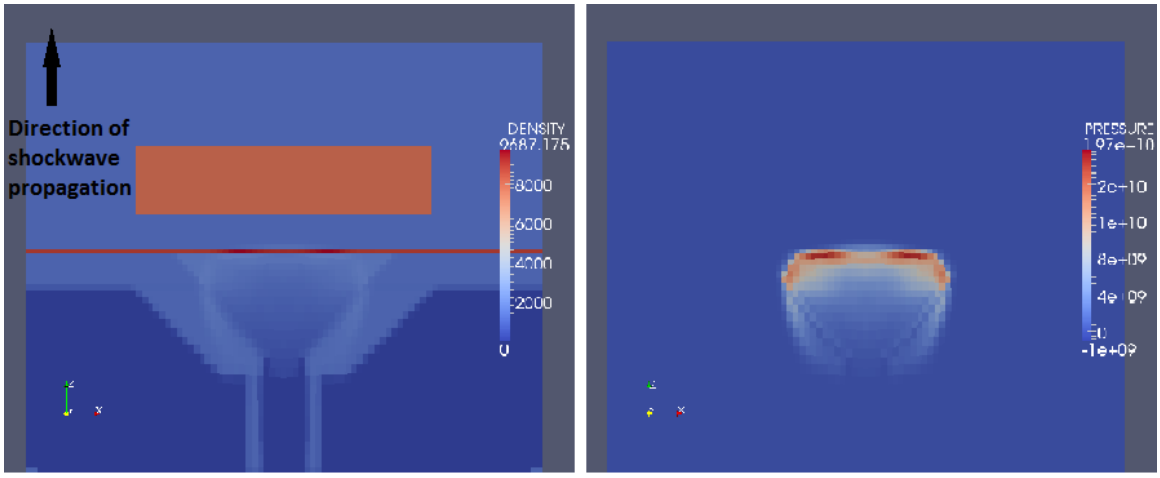

Density at shockwave impact on copper plate

Pressure at shockwave impact on copper plate

Figure 30. Visualization showing the wave front at impact of the copper plate. The left shows the density of the materials, the right shows the pressure front.

4.5 Scenario 2: 8 Blasting Cap Load

As mentioned previously, Circuit Model 1 (ideal resistor and ideal inductor in series) was used in the ALEGRA-EMMA environment to simulate the four 8-blasting cap cases. Table 7 shows a comparison of the simulation data rise time and peak values for voltage and Table 8 shows current for each of the cases as compared to the corresponding experimental values.

Table 7. Peak Voltages From 8-Blasting Cap Simulation.

Run Number	**Simulation Rise Time** μs	**Simulation Peak Voltage** $Volts$	**Experimental Rise Time** μs	**Experimental Peak Voltage** $Volts$
8 Cap-Case 1	0.325	3590	0.3383	7530
8 Cap-Case 2	0.388	5210	0.4210	8612
8 Cap-Case 3	0.325	4540	0.3707	7530
8 Cap-Case 4	0.325	4480	0.3667	7783

Table 8. Peak Current From 8-Blasting Cap Simulation.

Run Number	**Simulation Rise Time** μs	**Simulation Peak Current** $Amps$	**Experimental Rise Time** μs	**Experimental Peak Current** $Amps$
8 Cap-Case 1	1.822	-40.10	1.9082	-41.84
8 Cap-Case 2	1.288	-43.20	1.9141	-42.64
8 Cap-Case 3	1.228	-42.00	2.0464	-44.00
8 Cap-Case 4	1.228	-41.90	1.8981	-41.41

The simulation results for Case 1 as compared to the experimental data is shown in Figure 31. The data is plotted on a coincident time scale. Examining the current data, the lower graph in the figure, it can be seen that the simulation data for the current has approximately the same shape as the experimental data. The simulation also has the same initial slope as the experimental data, suggesting a good initial

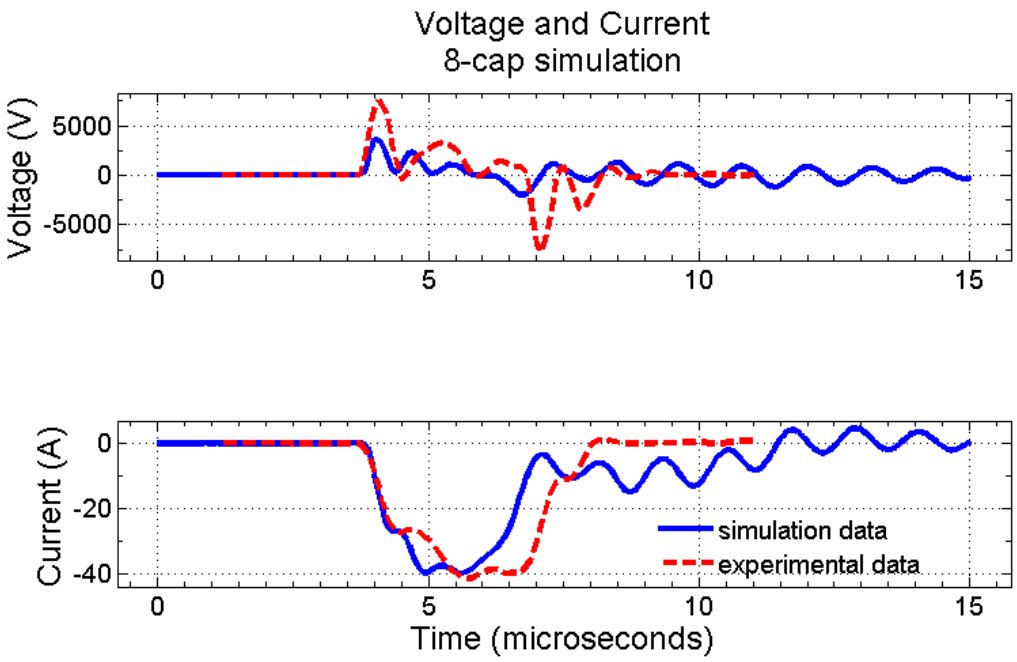

Figure 31. Case 1 - Plot showing comparison of ALEGRA-EMMA simulation to recorded experimental data of 8-blasting cap array.

match in data. From this comparison, it can also be seen that the peak value of the simulation is at approximately the same value as the experimental data, though not at the same time. In fact, the entire sequence of the reaction is on a shorter time scale than seen in the experimental data, though the general shape remains the same with three distinct negative-valued peaks. Another important distinction, after the reaction had concluded in the experimental data and the current returns to a zero value, the simulation data continued to show an oscillatory trend through the rest of the time frame of the simulation. Additional simulations with longer time frames show that the oscillations do have a damping trend, but it takes a relatively long time for this to occur.

Now looking at the voltage, the upper graph in Figure 31, the first thing to note is that the shape for the simulation data is also similar to the experimental data shape, though with the same compressed time scale that was seen in the current data. The

voltage simulation data also shows the same oscillatory behavior that was described in the current data. While able to match the simulation peak value data to the experimental data for the current, it is obvious that the voltage does not match the peak value height. A voltage mismatch clearly indicates that while the model chosen might be accurate for modeling the magnitude of the current, there is still work that needs to be done to make it accurate for the voltage as well.

This oscillatory behavior that is seen in both the voltage and the current could be due to any one or combination of several factors. The most likely cause could be a breakdown effect that occurs in the circuit in the actual experiments that can not occur in the simulation due to lack of a breakdown modeling capability. Any mechanism that could cause a break in the circuit in the experimental setup, whether it be ferroelectric breakdown or assembly break, would not be seen in modeling. The discrepancy could also be due to the fact that in the simulation, there are pockets of residual polarization that remain after the shock wave passes through the PZT material. Residual polarization can be seen in Figure 32 which shows the comparison of the polarization in the PZT block at the start of the simulation on the left and after the shock wave has passed through the material on the right. Polarization in the diagram is in Coloumbs/m^2. In theory, the block should be almost completely depolarized. Remaining polarization could be due to the fact that the plane wave generator output opening area is smaller than the PZT block face area that is exposed to the initial shockwave and the simulation may have difficulties with the mismatch. A small amount of remaining polarization in the simulation could potentially cause oscillations in the system. The oscillations could also be explained by noting that there are always losses in an actual system, energy dissipation that is not modeled in the simulated environment. The experimental setup included long lengths of wire connecting each of the blasting caps where potential dissipation could occur, where as

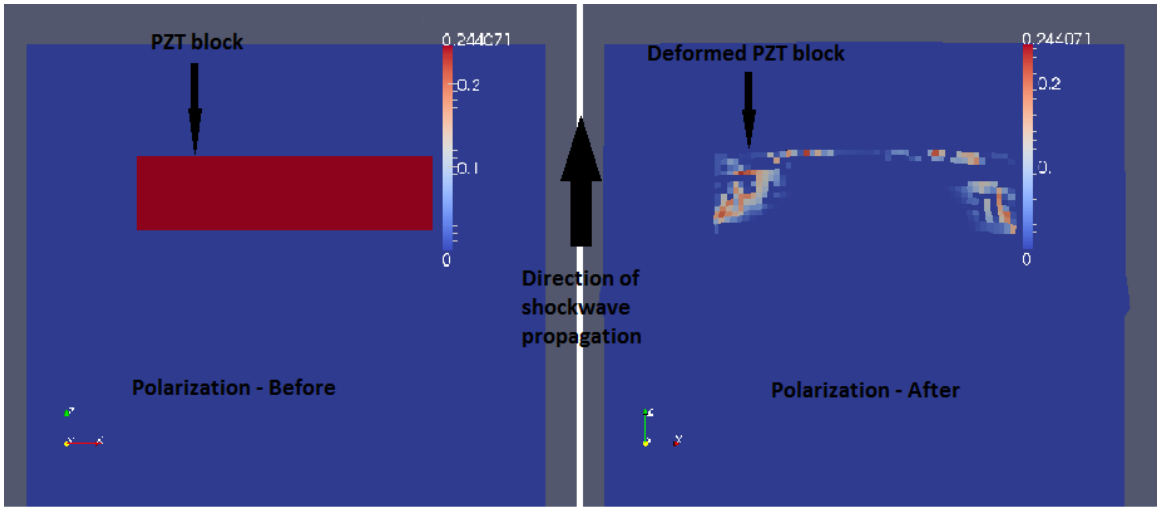

Figure 32. Comparison of PZT polarization before (left) and after (right) shock wave has passed through material.

the simulated model only includes nodes and ideal circuit elements and no dissipatory model.

The comparison of simulation to experimental data for Case 2 is shown in Figure 33. In both the current and the voltage plots, many of the same observations that were made about Case 1 can be made for Case 2. The simulation data peak value for the current matches fairly well to the experimental data while the voltage peak values does not. The voltage simulation data does show a higer peak value than Case 1, but this is likely due to the large difference in the inductance load of the circuit, as Case 1 and Case 2 are the lowest and highest experimental inductance values, respectively, and a higher inductance load will result in a higher voltage. The similar overall graph shape for both the current and voltage is also apparent. Case 2 also shows the same oscillatory behavior in the current and the voltage.

Figure 34 and Figure 35 show the comparison between the simulation and experimental data for Cases 3 and 4, respectively. Looking at the current and voltage plots, Cases 3 and 4 show the same general trends as the first two cases regarding the peak heights and time scale and the oscillatory nature of the simulation. Peak values for

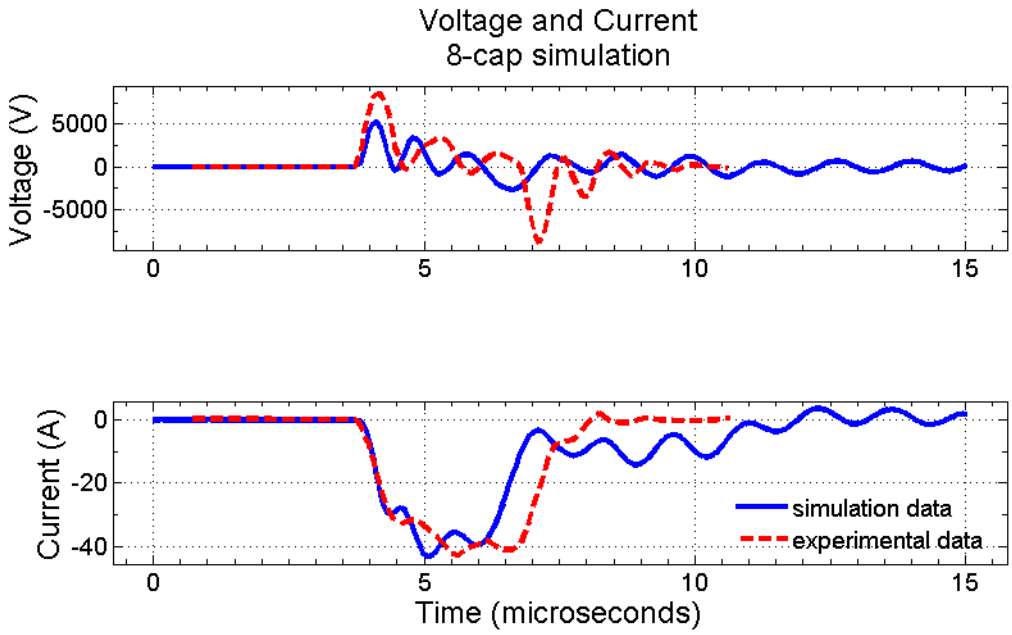

Figure 33. Case 2 - Plot showing comparison of ALEGRA-EMMA simulation to recorded experimental data of 8-blasting cap array.

the voltage and the current are very similar for these two cases, which is expected since the values for the inductance and resistance elements are very close for these two simulations.

4.6 Scenario 3: 64 Blasting Cap Load

Circuit Model 1 (ideal resistor and ideal inductor in series) was used in the ALEGRA-EMMA environment to simulate the three 64-blasting cap cases. Table 9 shows a comparison of the simulation data rise time and peak values for voltage and Table 10 shows current for each of the cases as compared to the corresponding experimental values.

Figure 36 shows the comparison of simulation to experimental data for the 64-blasting cap scenario, Case 1. Looking at the bottom plot shows the current data. For the comparison, only the experimental data up to the circuit breakdown point

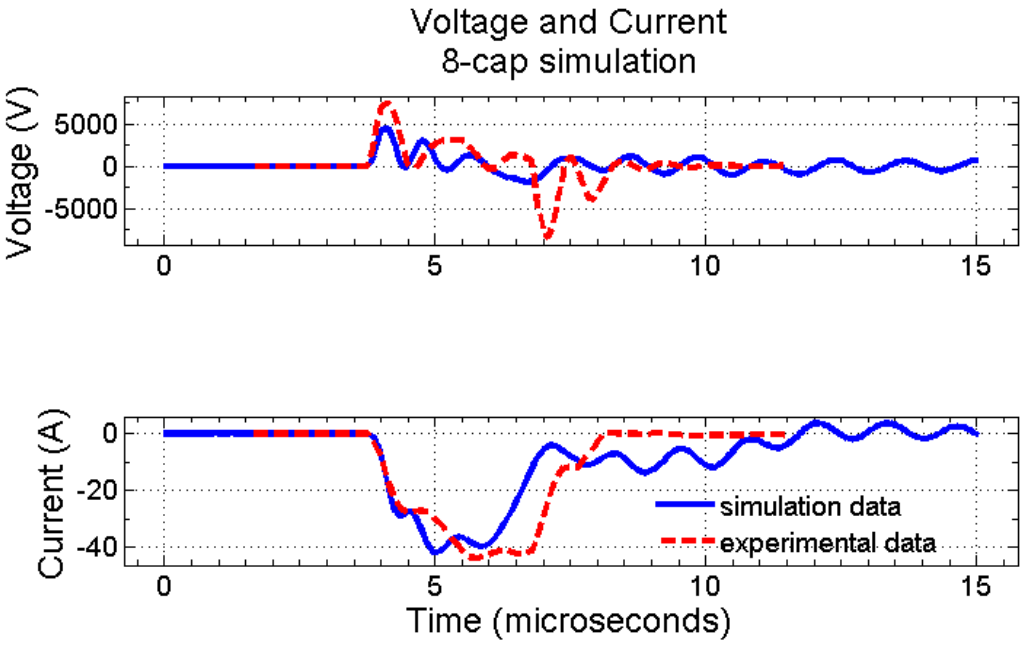

Figure 34. Case 3 - Plot showing comparison of ALEGRA-EMMA simulation to recorded experimental data of 8-blasting cap array.

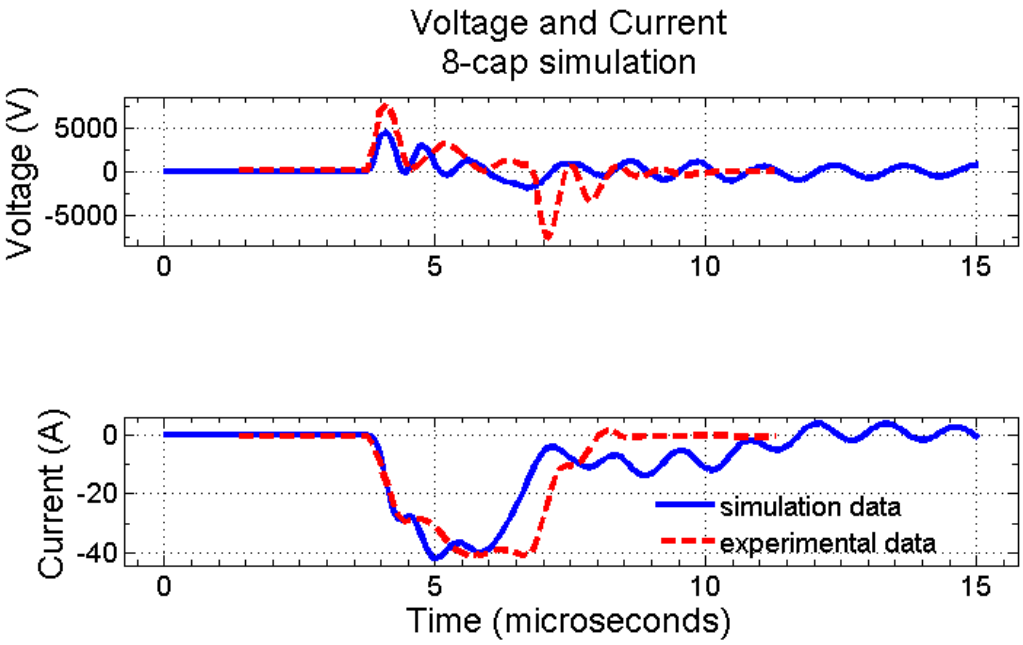

Figure 35. Case 4 - Plot showing comparison of ALEGRA-EMMA simulation to recorded experimental data of 8-blasting cap array.

Table 9. Peak Voltages From 64-Blasting Cap Simulation.

Run Number	**Simulation Rise Time** μs	**Simulation Peak Voltage** $Volts$	**Experimental Rise Time** μs	**Experimental Peak Voltage** $Volts$
64 Cap-Case 1	0.581	26,600	1.2397	10,380
64 Cap-Case 2	0.581	26,100	1.0370	15,100
64 Cap-Case 3	0.581	26,900	0.8992	18,100

Table 10. Peak Current From 64-Blasting Cap Simulation.

Run Number	**Simulation Rise Time** μs	**Simulation Peak Current** $Amps$	**Experimental Rise Time** μs	**Experimental Peak Current** $Amps$
64 Cap-Case 1	1.222	47.80	2.0727	41.71
64 Cap-Case 2	1.162	47.40	1.8786	44.98
64 Cap-Case 3	1.156	47.70	2.6960	46.47

at about 7.5 μs will be considered, as there is no breakdown in the simulation code. The overall shape of the simulation current with respect to the experimental data is similar, though the slope or speed of the reaction of the simulation data at the beginning of the reaction is higher than the experimental. As discussed above, the 8-blasting cap simulation matched the initial slope of the experimental data with much more accuracy. The peak value of the simulation data is slightly higher than the peak value of the experimental data.

Looking at the voltage now in the upper plot, it can be seen that the general shape of the simulation data is similar to the experimental data, though there is a large difference in the peak value of the voltage. As seen in comparing Table 7 to Table 9, there is much more variation in the peak experimental voltage heights in the 64-blasting cap scenario than in the 8-blasting cap scenario. While in the 8-blasting cap scenario the simulation voltage was lower than the experimental data in all four

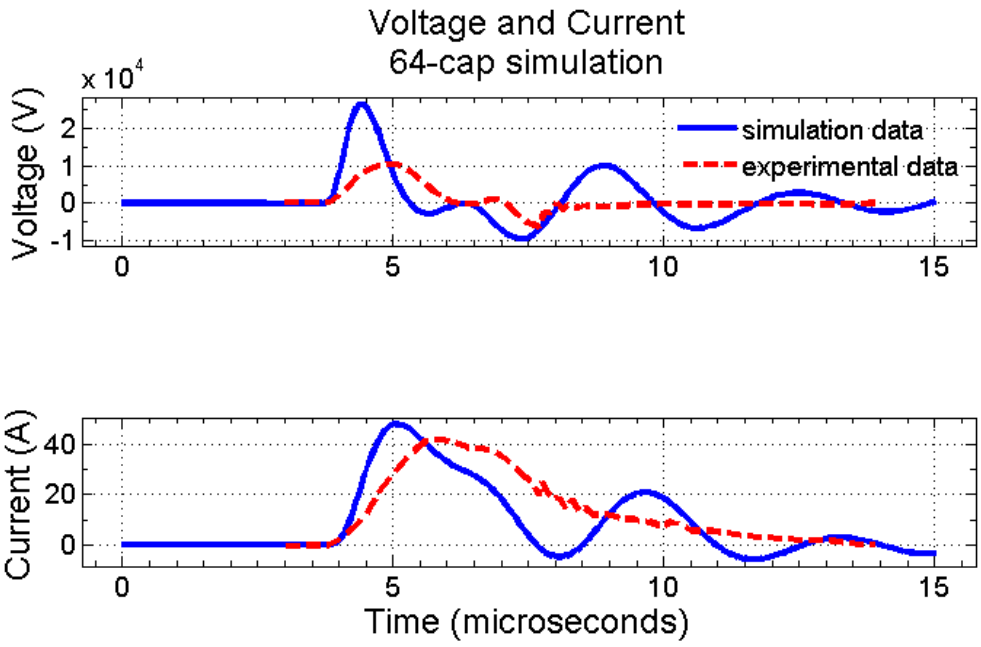

Figure 36. Case 1 - Plot showing comparison of ALEGRA-EMMA simulation to recorded experimental data of 64-blasting cap array.

cases, in the 64-blasting cap scenario the peak simulation voltage is higher than the experimental in all three cases. As in the current data, the slope of the simulation voltage data is also higher than the experimental data at the beginning of the reaction.

Similar results are seen in Figure 37, which shows the comparison of Case 2 data. The general shape of both the simulation voltage and current match the experimental data. The same observations can be made about the peak values for the current and the voltage.

Figure 38 shows the comparison of Case 3 data. In dealing with Cases 1 and 2, it can be noted that the general shape of the plots for both the voltage and the current are similar. Comparing Cases 1 and 2 to the plots for Case 3, the shapes of the graphs of both parameters are different. As discussed in Chapter 2, the dissimilarity could be due to any number of anomalies in the experimental setup or perhaps due to differences in the blasting caps used for the specific test. Comparing the simulation results to the experimental data for Case 3 will clearly not show a similarity in

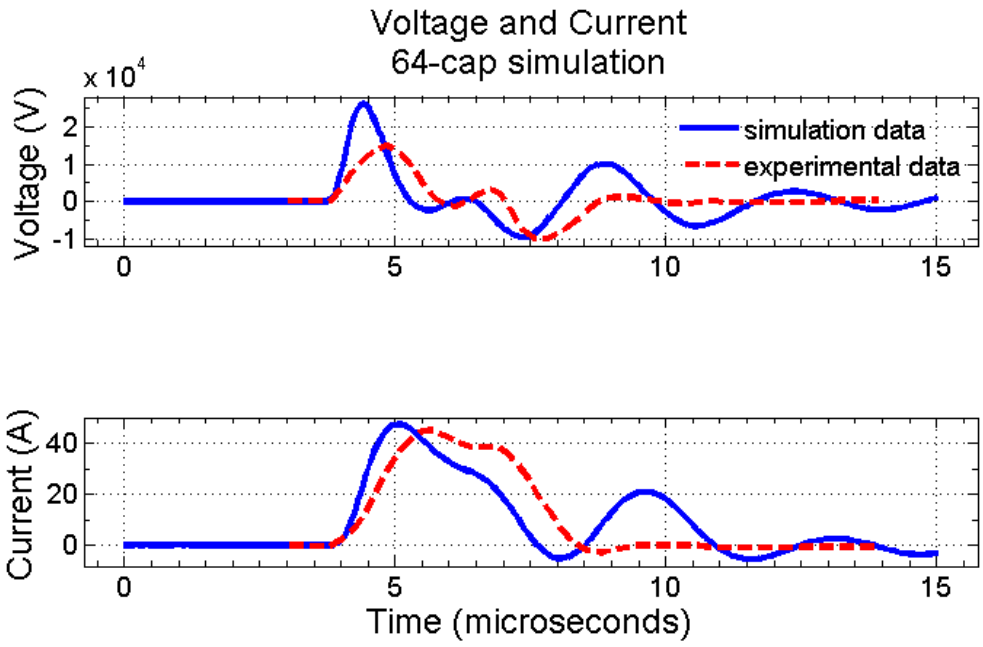

Figure 37. Case 2 - Plot showing comparison of ALEGRA-EMMA simulation to recorded experimental data of 64-blasting cap array.

shape for either the current or the voltage, as was seen in the previous two cases. However, it can be noted that while the shapes are different, the peak value recorded for the current is very close to the simulation current peak value. As in the previous cases discussed above, the voltage values for the simulation still do not match the experimental data.

The same shortening of the time scale that was seen in the 8-blasting cap scenario can be seen in the current and the voltage for Cases 1 through 3. Additionally, the oscillatory behavior that was present in the simulation data for the 8-cap scenario is seen in all three cases of the 64-cap scenario as well. The same possible explanations that were discussed above can be applied to the 64-cap scenario as well.

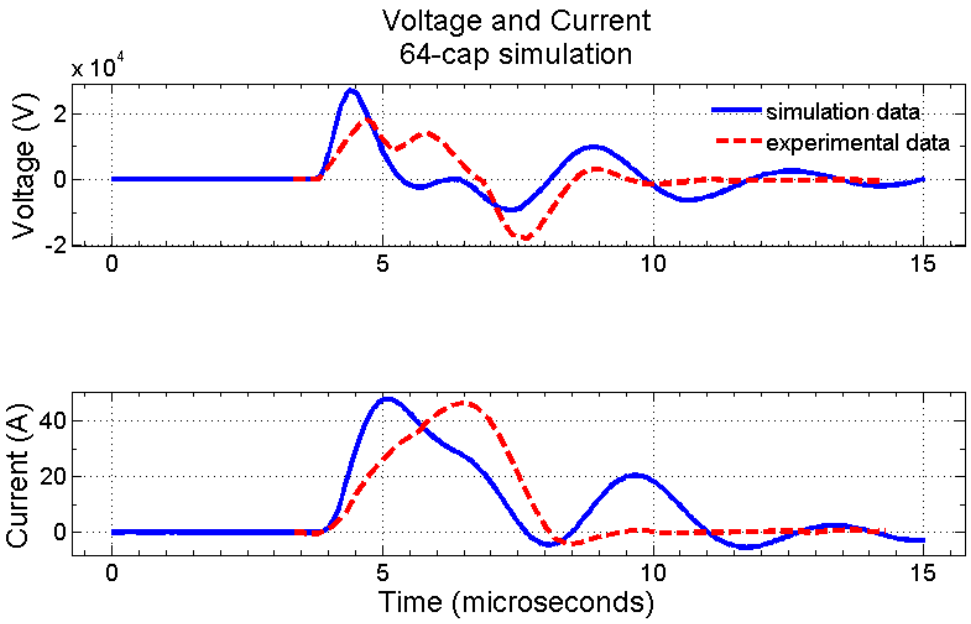

Figure 38. Case 3 - Plot showing comparison of ALEGRA-EMMA simulation to recorded experimental data of 64-blasting cap array.

V. Conclusions and Recommendations

5.1 Chapter Overview

This chapter contains two sections that summarize the results from the ALEGRA-EMMA model output for each case study and provides recommendations for future work with both the ALEGRA model as well as future experimental work.

5.2 Conclusions

There are several results that were discussed in Chapter 4 that are important to summarize in the discussion and evaluation of the simulation model. In both of the closed circuit scenarios, the model was able to fairly accurately represent the general shape of both the current and the voltage. Though the ALEGRA code is unable to simulate breakdown, as is seen in the open circuit cases, the model worked fairly well to predict the peak current values in both scenarios, though the simulated voltage values in the 8-blasting cap scenario were consistently lower than experimental while the simulated values for the 64-blasting cap scenario were consistently higher than the experimental data. The model also resulted in a consistent shorter time scale of the reaction as compared to the experimental data across all seven cases. The closed circuit cases all showed an oscillatory nature after the reaction should have been completed and the experimental data showed the circuit returning to a zero value for both the current and the voltage. In all cases, the oscillations show a decaying trend over time, suggesting that they will eventually decay to zero.

One difference that occurs between the scenarios, while in the 8-blasting cap scenario the initial reaction in the simulation matches the experimental data as far as the slopes of the current data, in the 64-blasting cap and the open circuit scenario the slopes start the same, but the simulation quickly outpaces the experimental data

and achieves a higher slope, in the voltage and in the current (where applicable).

Overall, these results suggest that the model developed could be used as a way to predict the current peak value and general plot shape that would be produced from a designed circuit load using the Redstone PZT formulation. The model could also be used to predict the general shape of the voltage data but requires a more in-depth study of the PZT model parameters in order to accurately determine the peak voltages that would be produced by the same setup.

5.3 Recommendations for Future Work

Future work that would help further this research would be a more detailed look at the material parameters that define the PZT block in the ALEGRA-EMMA code simulation. A higher fidelity optimization would likely need to be performed that takes into account more of the parameter variables and that would be able to handle the complex, interrelated process of varying those parameters. One method of doing this would be to incorporate a code called DAKOTA (11), developed by Sandia National Laboratories. DAKOTA is an optimization and uncertainty analysis code that can be integrated with a simulation model code and used to explore the complex nature of the system being modeled. The code can be used for design optimization, uncertainty quantification, sensitivity analysis, calibration, and as a verification and validation tool through iterative analytical techniques.

While currently the DAKOTA code would need to be incorporated externally to the ALEGRA-EMMA environment, future versions of the ALEGRA-EMMA code are planned to include a method of internally interfacing with DAKOTA that makes the analysis more streamlined.

The next addition and area of future research that would be of great value to the model would be breakdown modeling capability, something that would need to

be incorporated into the ALEGRA-EMMA code itself, not just the simulation model input deck. Many more years of work would be required to incorporate this type of addition. In the near term, potential solutions to the breakdown problem could be to try and incorporate a non-linear permittivity model for the ferroelectric material that could produce similar results to that of breakdown. Another area to look at would be incorporating time varying circuit elements that could be used to break the circuit, as would happen if breakdown were to occur in the ferroelectric material.

Appendix A. Appendix A: FEG Engineering Schematics

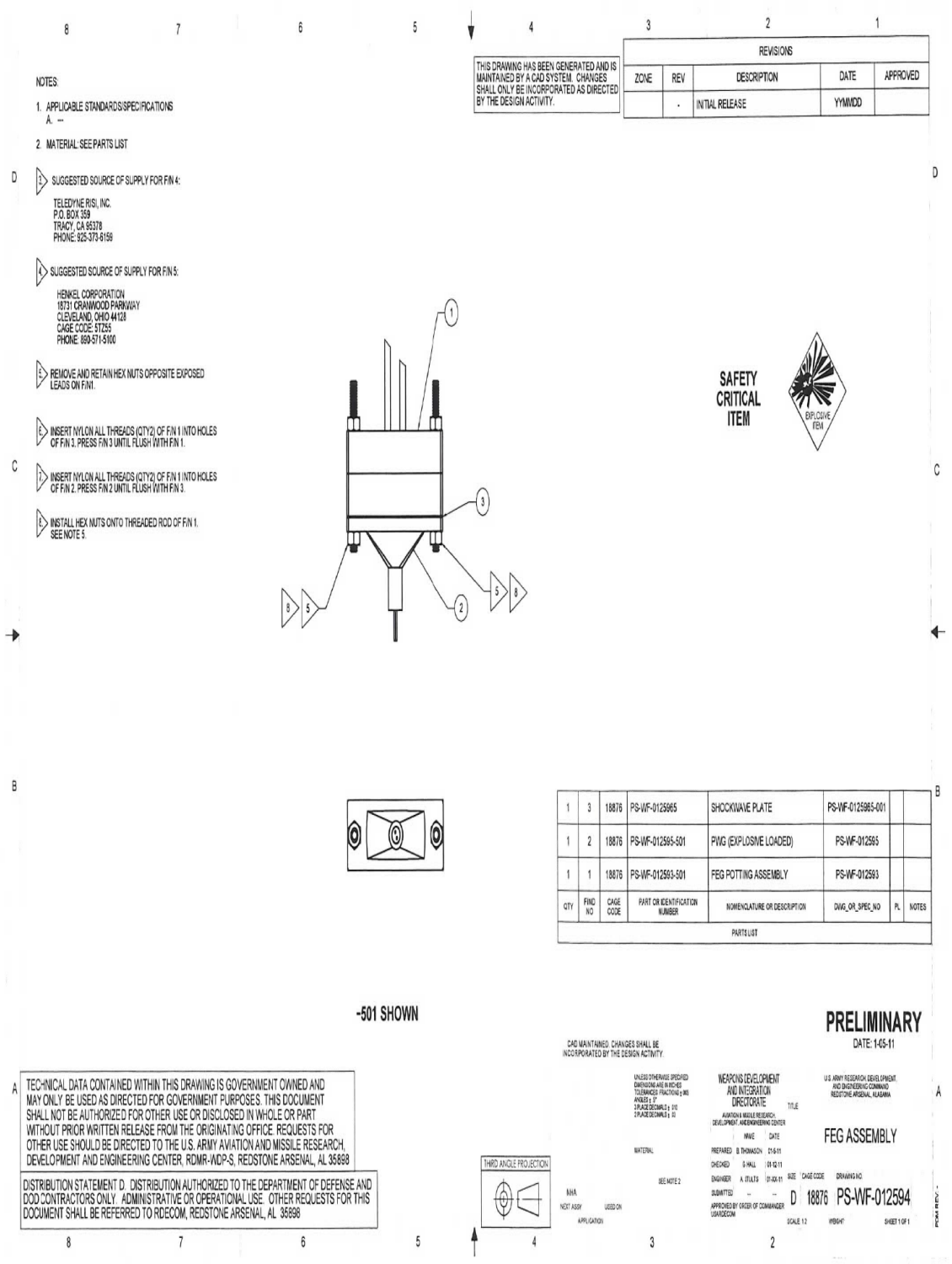

Figure 39. Redstone FEG Engineering Schematic - View 1.

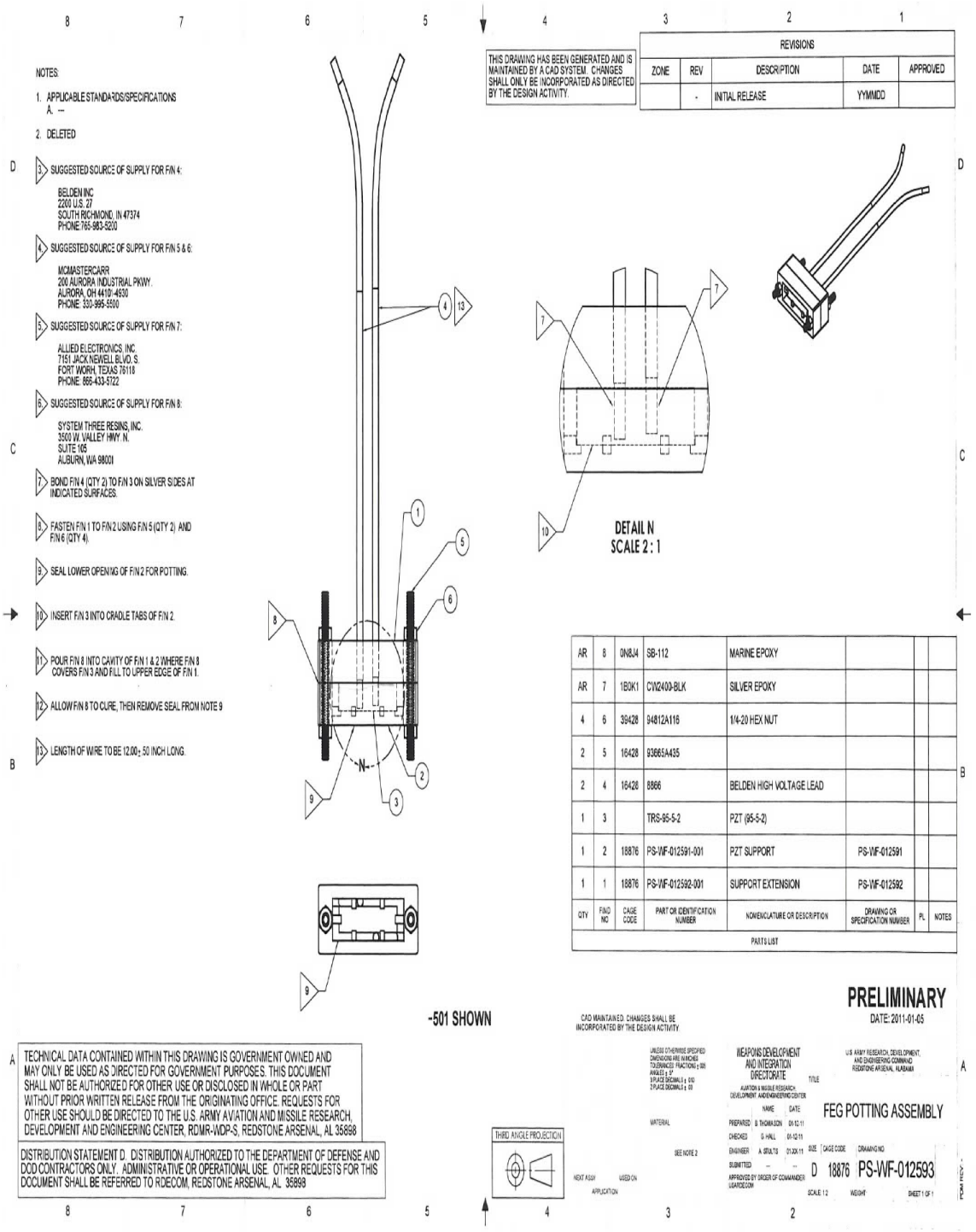

Figure 40. Redstone FEG Engineering Schematic - View 2.

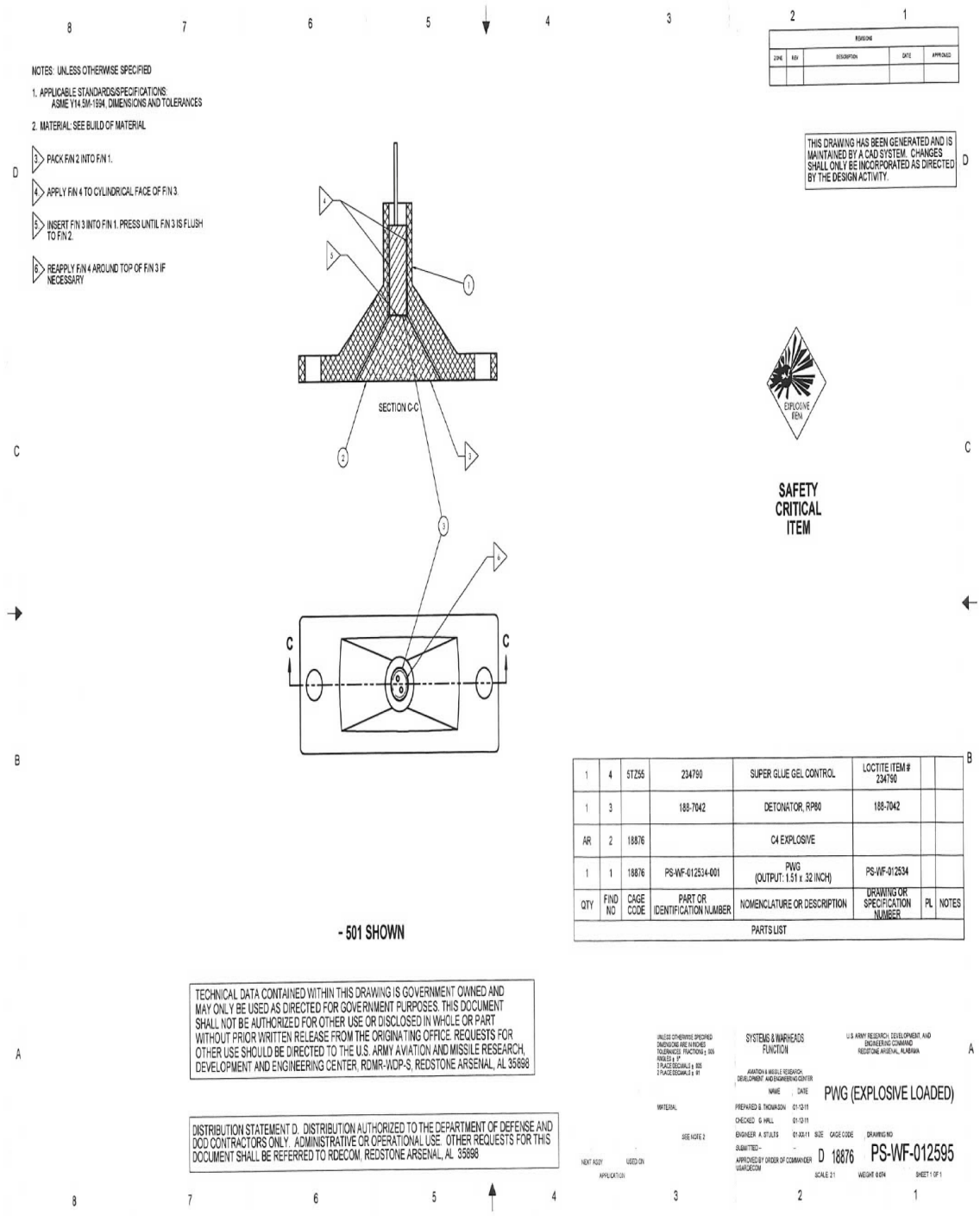

Figure 41. Redstone FEG Engineering Schematic - View 3.

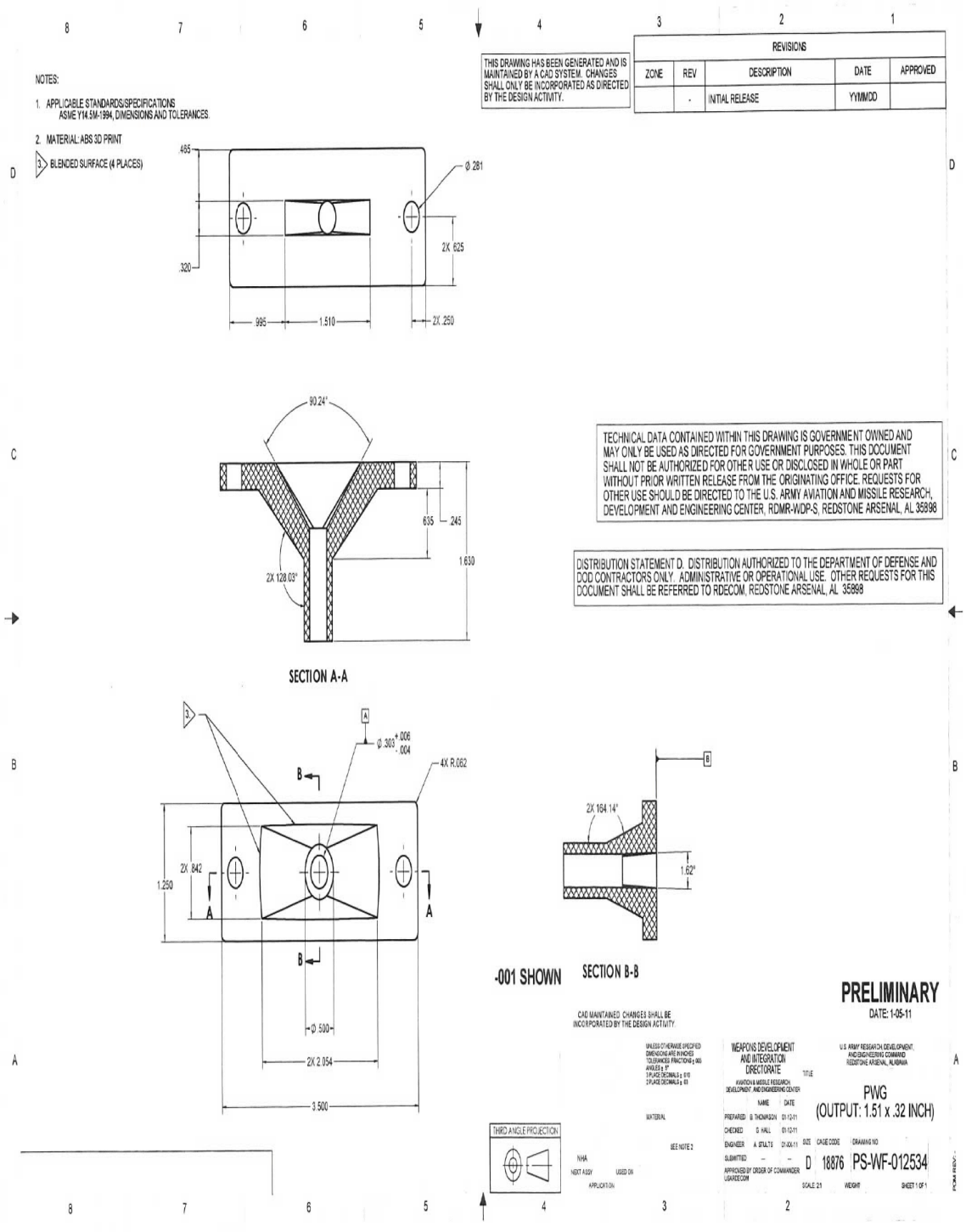

Figure 42. Redstone FEG Engineering Schematic - View 4.

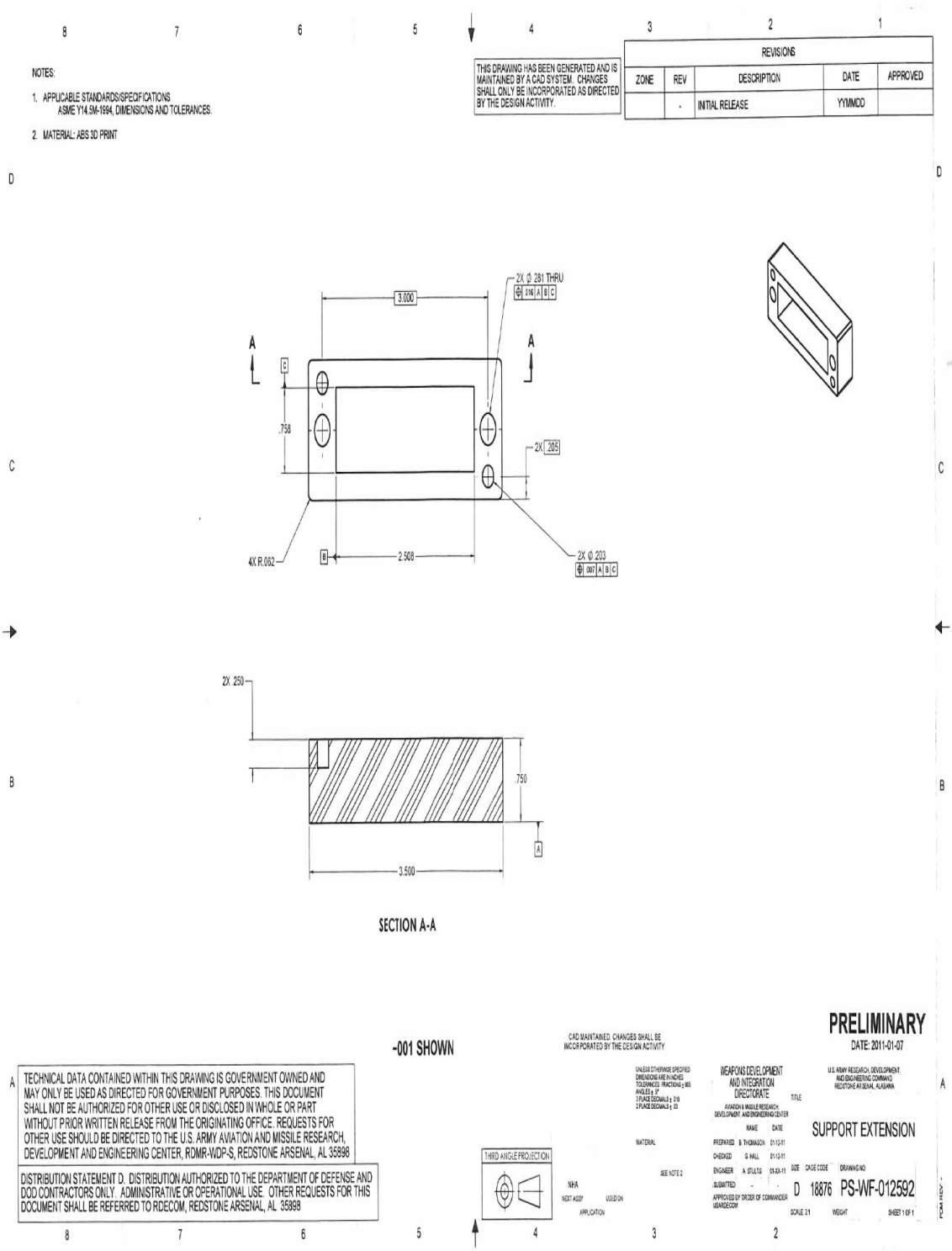

Figure 43. Redstone FEG Engineering Schematic - View 5.

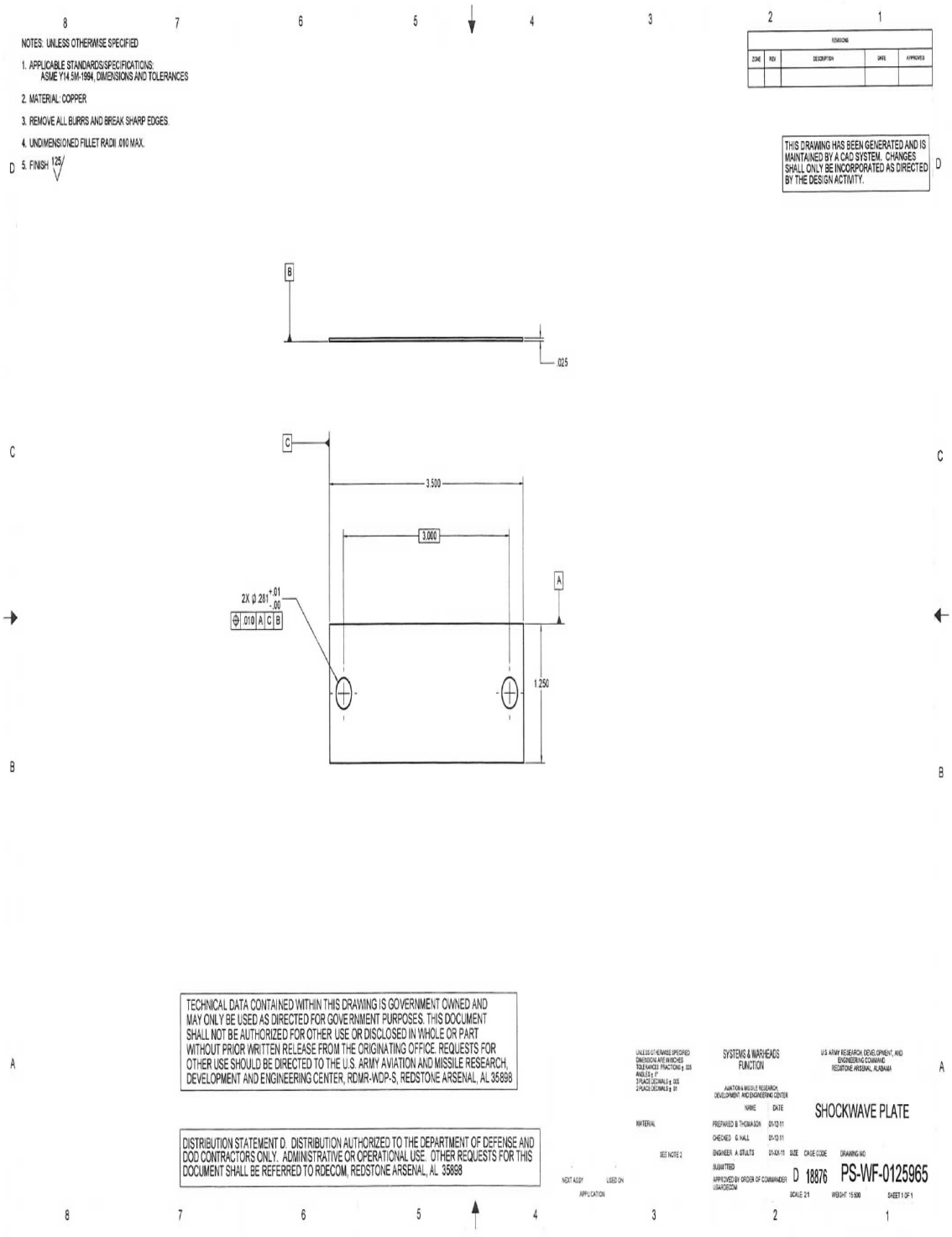

Figure 44. Redstone FEG Engineering Schematic - View 6.

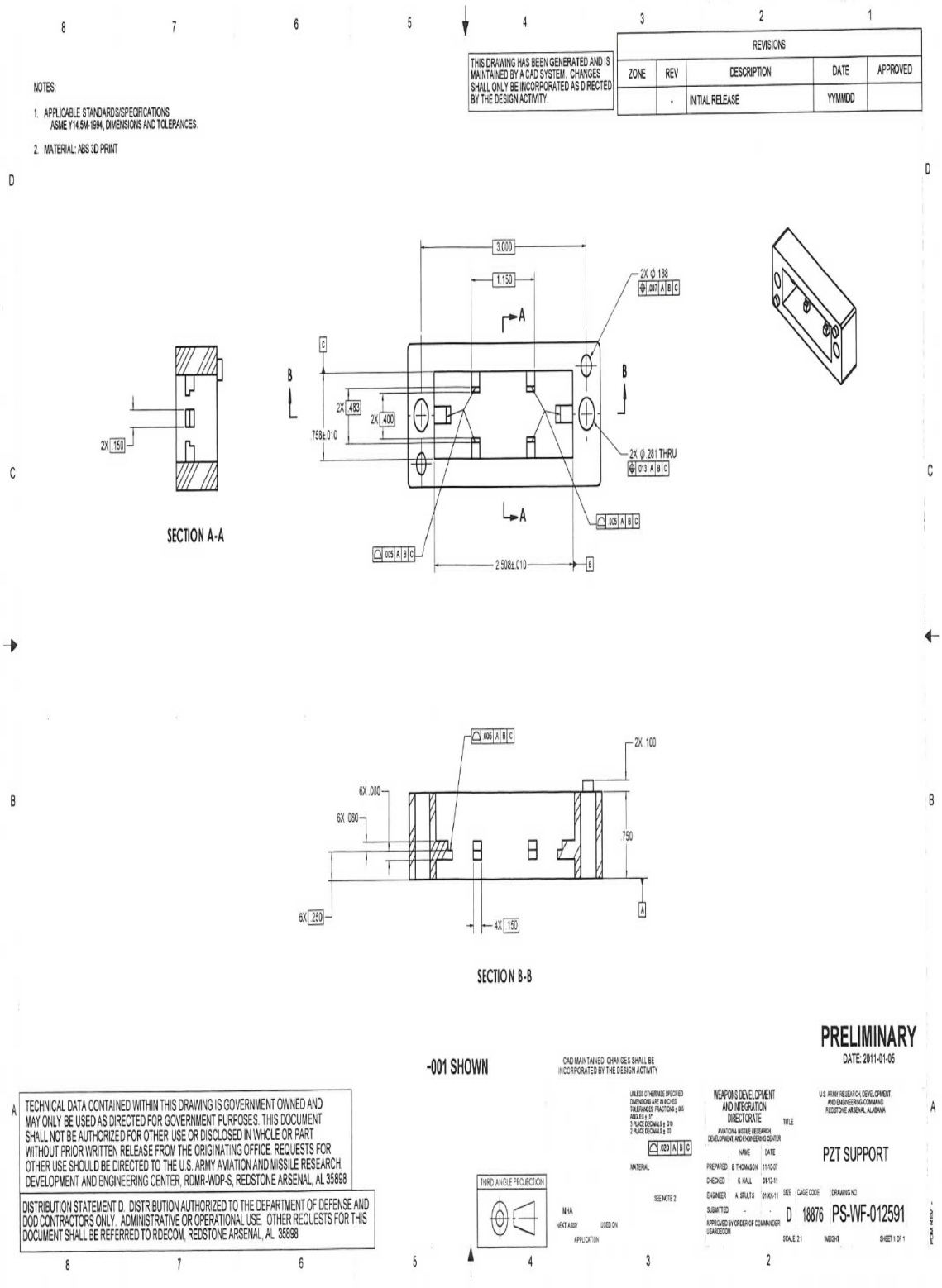

Figure 45. Redstone FEG Engineering Schematic - View 7.

Appendix B. Appendix B: MATLAB Circuit Model Differential Equation Scripts

This first script shows the code used to solve for Circuit Model 1.

```
%%%%-------------------------------------------------------------------------%%%%
close all; clear all; clc;
%%%% Difeq circuit 1 - simple non-ideal inductor, series %%%%

%%% Identify filename - experimental data
     [filename, pathname] = uigetfile( ...
         {'*.dat;', ...
        'All MATLAB DAT Files (*.dat)'; ...
        '*.*', ...
        'All Files (*.*)'}, ...
           'Select current data file');
     if isequal(filename,0) | isequal(pathname,0)
      return
     else
      imagename = fullfile(pathname, filename);
     end
%%% import the data file with current
reply = filename;
M = importdata(reply,' ');
[row,col] = size(M);
fid = fopen(reply);
data = M;
current = data(:,2);
% current = smooth(current);
time_c = data(:,1).*10^(-6);
```

```
%%% Identify filename - experimental data
     [filename, pathname] = uigetfile( ...
         {'*.dat;', ...
        'All MATLAB DAT Files (*.dat)'; ...
        '*.*', ...
        'All Files (*.*)'}, ...
           'Select voltage data file');
     if isequal(filename,0) | isequal(pathname,0)
      return
     else
      imagename = fullfile(pathname, filename);
     end
%%% import the data file with voltage
reply = filename;
M = importdata(reply,' ');
[row,col] = size(M);
fid = fopen(reply);
data = M;
volt = data(1:end,2);
% volt = smooth(volt);
time_v = data(1:end,1).*10^(-6);


%%% values for circuit elements

% %%%% 8 cap
% L = 51.6*10^(-6);      % Henries
% R = 15.9;              % Ohms

% %%%% 64 cap
L = 348.8*10^(-6);      % Henries
R = 115;              % Ohms
```

```
current = -current;

%%% differential equations to find voltage
Vr = current(1:end-1).*R;
Vr = smooth(Vr);
Vl = L.*(diff(current))./(diff(time_c));
Vl = smooth(Vl);

voltage = -(Vr + Vl);
time_dl = time_c(1:end-1);

[exp_max_v,vi] = max(volt);
exp_rise_v = (time_v(vi)-time_v(2))*10^6;
fprintf('------------ Experimental data ------------ \n')
fprintf('voltage rise time is: %0.4f microseconds \n',exp_rise_v)
fprintf('max is: %0.3d \n',exp_max_v)
[exp_max_c,ci] = min(current);
exp_rise_c = (time_c(ci)-time_c(2))*10^6;
fprintf('current rise time is: %0.4f microseconds \n',exp_rise_c)
fprintf('min is: %0.3d \n',exp_max_c)
fprintf('------------------------ \n')

%%% 64 cap
current = -current;

figure
h = subplot(2,1,1);
plot(time_dl.*10^6,voltage,'--r','Linewidth',3)
% set(gca,'YTickLabel',num2str(get(gca,'YTick').'))
hold on
ylabel('Voltage (V)')
plot(time_v.*10^6,volt,'-b','Linewidth',3)
```

```
legend('calc. data','exp. data','Location','Best')
title({'Experimental Data - Circuit Model Prediction';...
    'Voltage and Current vs. Time'})
hold on
grid on
prettyPlot('axis',h,'AxisTight',true,'pct',5,'MinorTicks',true,...
                    'FontSize',14,'FontName',[],'Format',true,...
                    'SetSize',true,'Width',11,'AspectRatio',600/1024);
h = subplot(2,1,2);
plot(time_c.*10^6,current,'-b','Linewidth',3)
% set(gca,'YTickLabel',num2str(get(gca,'YTick').'))
% axis([10 20 -150 20])
axis([10 20 -60 20])
ylabel('Current (A)')
xlabel('Time (microseconds)')
grid on
prettyPlot('axis',h,'AxisTight',true,'pct',5,'MinorTicks',true,...
                    'FontSize',14,'FontName',[],'Format',true,...
                    'SetSize',true,'Width',11,'AspectRatio',600/1024);
%%%%-------------------------------------------------------------------------%%%%
```

This second script shows the code used to solve for Circuit Model 2.

```
%%%%-------------------------------------------------------------------------%%%%
close all; clear all; clc;
%%%% Difeq circuit 2 - complex non-ideal inductor %%%%

%%% Identify filename - experimental data
     [filename, pathname] = uigetfile( ...
         {'*.dat;', ...
        'All MATLAB DAT Files (*.dat)'; ...
```

```
        '*.*', ...
        'All Files (*.*)'}, ...
           'Select current data file');
     if isequal(filename,0) | isequal(pathname,0)
      return
     else
      imagename = fullfile(pathname, filename);
     end
%%% import the data file with current
reply = filename;
M = importdata(reply,' ');
[row,col] = size(M);
fid = fopen(reply);
data = M;
current = data(:,2);
% current = smooth(current);
time_c = data(:,1).*10^(-6);


%%% Identify filename - experimental data
     [filename, pathname] = uigetfile( ...
         {'*.dat;', ...
        'All MATLAB DAT Files (*.dat)'; ...
        '*.*', ...
        'All Files (*.*)'}, ...
           'Select voltage data file');
     if isequal(filename,0) | isequal(pathname,0)
      return
     else
      imagename = fullfile(pathname, filename);
     end
%%% import the data file with voltage
```

```
reply = filename;
M = importdata(reply,' ');
[row,col] = size(M);
fid = fopen(reply);
data = M;
volt = data(1:end,2);
% volt = smooth(volt);
time_v = data(1:end,1).*10^(-6);


%%% values for circuit elements

% %%%% 8 cap
% L = 51.6*10^(-6);      % Henries
% Ca = 145*10^(-12);   % Farads
% R = 15.9;              % Ohms

% %%%% 64 cap
L = 348.8*10^(-6);      % Henries
Ca = 145*10^(-12);
R = 115;              % Ohms
current = -current;

%%% ODE to find i1
[T,i1] = ode45(@(t,i1) circuit_current(t,i1,current,L,R,Ca,time_c),...
    time_c,[0 0]);
i1 = smooth(i1(:,1));
i2 = (current-i1(:,1));
% i2 = smooth(i2);

Vr = i1(1).*R;
Vr = smooth(Vr);
```

```
Vl = L.*(diff(i1(:,1))./diff(time_c));
Vl = smooth(Vl);
voltage = -(Vr + Vl);
time_dl = time_c(1:end-1);

[exp_max_v,vi] = max(volt);
exp_rise_v = (time_v(vi)-time_v(2))*10^6;
fprintf('------------ Experimental data ------------ \n')
fprintf('voltage rise time is: %0.4f microseconds \n',exp_rise_v)
fprintf('max is: %0.3d \n',exp_max_v)
[exp_max_c,ci] = min(current);
exp_rise_c = (time_c(ci)-time_c(2))*10^6;
fprintf('current rise time is: %0.4f microseconds \n',exp_rise_c)
fprintf('min is: %0.3d \n',exp_max_c)
fprintf('------------------------ \n')

%%% 64 cap
current = -current;

figure
h = subplot(2,1,1);
plot(time_dl.*10^6,voltage,'--r','Linewidth',3)
% set(gca,'YTickLabel',num2str(get(gca,'YTick').'))
hold on
ylabel('Voltage (V)')
plot(time_v.*10^6,volt,'-b','Linewidth',3)
legend('calc. data','exp. data','Location','Best')
title({'Experimental Data - Circuit Model Prediction';...
    'Voltage and Current vs. Time'})
hold on
grid on
prettyPlot('axis',h,'AxisTight',true,'pct',5,'MinorTicks',true,...
```

```
                    'FontSize',14,'FontName',[],'Format',true,...
                    'SetSize',true,'Width',11,'AspectRatio',600/1024);
h = subplot(2,1,2);
plot(time_c.*10^6,current,'-b','Linewidth',3)
% set(gca,'YTickLabel',num2str(get(gca,'YTick').'))
% axis([10 20 -150 20])
% axis([10 20 -60 20])
ylabel('Current (A)')
xlabel('Time (microseconds)')
grid on
prettyPlot('axis',h,'AxisTight',true,'pct',5,'MinorTicks',true,...
                    'FontSize',14,'FontName',[],'Format',true,...
                    'SetSize',true,'Width',11,'AspectRatio',600/1024);
%%%%-------------------------------------------------------------------------%%%%
```

This function is the differential equation solver function associated with Circuit Model 2.

```
function di1 = circuit(t,i1,current,L,R,Ca,time)
di1 = zeros(2,1);
it = interp1(time,current,t);

di1(1) = i1(2);
di1(2) = it./(L*Ca) - i1(1)./(L*Ca) - R./L.*i1(2);
%%%%-------------------------------------------------------------------------%%%%
```

This third script shows the code used to solve for Circuit Model 3.

```
%%%%-------------------------------------------------------------------------%%%%
close all; clear all; clc;
%%%% Difeq circuit 3 - simple non-ideal inductor, parallel %%%%
```

```
%%% Identify filename – experimental data
     [filename, pathname] = uigetfile( ...
         {'*.dat;', ...
        'All MATLAB DAT Files (*.dat)'; ...
        '*.*', ...
        'All Files (*.*)'}, ...
           'Select current data file');
     if isequal(filename,0) | isequal(pathname,0)
      return
     else
      imagename = fullfile(pathname, filename);
     end
%%% import the data file with current
reply = filename;
M = importdata(reply,' ');
[row,col] = size(M);
fid = fopen(reply);
data = M;
current = data(:,2);
% current = smooth(current);
time_c = data(:,1).*10^(-6);


%%% Identify filename – experimental data
     [filename, pathname] = uigetfile( ...
         {'*.dat;', ...
        'All MATLAB DAT Files (*.dat)'; ...
        '*.*', ...
        'All Files (*.*)'}, ...
           'Select voltage data file');
     if isequal(filename,0) | isequal(pathname,0)
```

```
      return
     else
      imagename = fullfile(pathname, filename);
     end
%%% import the data file with voltage
reply = filename;
M = importdata(reply,' ');
[row,col] = size(M);
fid = fopen(reply);
data = M;
volt = data(1:end,2);
% volt = smooth(volt);
time_v = data(1:end,1).*10^(-6);


%%% values for circuit elements

% %%%% 8 cap
% L = 51.6*10^(-6);      % Henries
% R = 15.9;              % Ohms

% %%%% 64 cap
L = 348.8*10^(-6);      % Henries
R = 115;               % Ohms
current = -current;

%%% ODE to find i1
[T,i1] = ode45(@(t,i1) circuit_current2(t,i1,current,L,R,time_c),...
    time_c,0);
i1 = smooth(i1);
i2 = (current-i1);
% i2 = smooth(i2);
```

```
Vr = i2.*R;
Vr = smooth(Vr);
Vl = L.*(diff(i1)./diff(time_c));
Vl = smooth(Vl);
voltage = -Vr(1:end-1);
% voltage = -Vl;
time_dl = time_c(1:end-1);

[exp_max_v,vi] = max(volt);
exp_rise_v = (time_v(vi)-time_v(2))*10^6;
fprintf('---------- Experimental data ---------- \n')
fprintf('voltage rise time is: %0.4f microseconds \n',exp_rise_v)
fprintf('max is: %0.3d \n',exp_max_v)
[exp_max_c,ci] = min(current);
exp_rise_c = (time_c(ci)-time_c(2))*10^6;
fprintf('current rise time is: %0.4f microseconds \n',exp_rise_c)
fprintf('min is: %0.3d \n',exp_max_c)
fprintf('------------------------ \n')

%%% 64 cap
current = -current;

figure
h = subplot(2,1,1);
plot(time_dl.*10^6,voltage,'--r','Linewidth',3)
% set(gca,'YTickLabel',num2str(get(gca,'YTick').'))
hold on
ylabel('Voltage (V)')
plot(time_v.*10^6,volt,'-b','Linewidth',3)
legend('calc. data','exp. data','Location','Best')
title({'Experimental Data - Circuit Model Prediction';...
```

```
    'Voltage and Current vs. Time'})
hold on
grid on
prettyPlot('axis',h,'AxisTight',true,'pct',5,'MinorTicks',true,...
                    'FontSize',14,'FontName',[],'Format',true,...
                    'SetSize',true,'Width',11,'AspectRatio',600/1024);
h = subplot(2,1,2);
plot(time_c.*10^6,current,'-b','Linewidth',3)
% set(gca,'YTickLabel',num2str(get(gca,'YTick').'))
% axis([10 20 -150 20])
% axis([10 20 -60 20])
ylabel('Current (A)')
xlabel('Time (microseconds)')
grid on
prettyPlot('axis',h,'AxisTight',true,'pct',5,'MinorTicks',true,...
                    'FontSize',14,'FontName',[],'Format',true,...
                    'SetSize',true,'Width',11,'AspectRatio',600/1024);
%%%%-------------------------------------------------------------------------%%%%
```

This function is the differential equation solver function associated with Circuit Model 3

```
function di1 = circuit_current2(t,i1,current,L,R,time)
% di1 = zeros(1,1);
it = interp1(time,current,t);

di1 = (it-i1).*(R/L);
%%%%-------------------------------------------------------------------------%%%%
```

Bibliography

1. "Ferroelectric and Peizoelectric Properties of NKN". World Wide Web Page. Available at *http://groups.ist.utl.pt/rschwarz/rschwarzgroup_files/Ferroelectrics_files/NOLEAD4.html*.

2. "Paraview User's Guide (v3.10)". Downloadable Users Manual. Available at *http://www.paraview.org/*.

3. *Lagrangian Continuum Dynamics in ALEGRA*. Technical Report SAND2007-8104, Sandia National Laboratories, 2007.

4. *Explosive Pulsed Power: An Enabling Technology*. Technical report, US Army Space and Missile Defense Command, 2008.

5. Altgilbers, L. et al. "Recent Advances in Explosive Pulsed Power". *Journal of Directed Energy*, 83:1–43, 2009.

6. Altgilbers, L. et al. *Explosive Pulsed Power*. Imperial College Press, London, England, 2011.

7. Donea, J. et al. "Arbitrary Lagrangian-Eulerian Methods". Erwin et al. Stein (editor), *Encyclopedia of Computational Mechanics*, 1–21. John Wiley and Sons, Ltd., 2004.

8. Moulson, A. and J. Herbert. *Electroceramics, 2nd Edition*. John Wiley and Sons, Ltd., West Sussex, England, 2003.

9. Robinson, Allen C. et al. "ALEGRA: An Arbitrary Lagrangian-Eulerian Multimaterial, Multiphysics Code". presented to *AIAA Aerospace Sciences Meeting and Exhibit*, January 2008.

10. Sandia National Laboratories, Sandia National Laboratories, Livermore, CA 94551. *CUBIT 13.2 User Documentation*, March 2012. Available at *http://cubit.sandia.gov/index.html*.

11. Sandia National Laboratories, Sandia National Laboratories, Livermore, CA 94551. *Dakota, A Multilevel Parallel Object-Oriented Framework for design Optimization, Parameter Estimation, Uncertainty Quantification and Sensitivity Analysis*, January 2013. Available at *http://dakota.sandia.gov/documentation.html*.

12. Setchell, Robert E. "Shock wave compression of the ferroelectric ceramic $Pb_{0.99}(Zr_{0.95}Nb_{0.02})_{0.98}Nb_{0.02}O_3$: Hugoniot states and constitutive mechanical properties". *Journal of Applied Physics*, 94, 2003.

13. Setchell, Robert E. "Shock wave compression of the ferroelectric ceramic $Pb_{0.99}(Zr_{0.95}Nb_{0.02})_{0.98}Nb_{0.02}O_3$: Depoling currents". *Journal of Applied Physics*, 97, 2005.

14. Shkuratov, S. et al. "Electric breakdown of longitudinally shocked $Pb(Zr_{0.52}Ti_{0.48})O_3$ ceramics". *Journal of Applied Physics*, 110, 2011.

15. Stults, Allen H. "Ferroelectric Generator Design for Multiple Initiation of Blasting Caps". presented to *IEEE International Pulsed Power Conference*, June 2011.

Vita

Captain Mollie Drumm was born in Grand Rapids, Michigan. After graduating from Forest Hills Central High School in 2002, she studied Aerospace Engineering at the University of Notre Dame. She graduated with a Bachelor of Science Degree in Aerospace Engineering in May 2006. After attending Air Force Officer Training School, she commissioned into the United States Air Force as a distinguished graduate in March 2007.

Captain Drumm's initial assignment upon commissioning was to Edwards Air Force Base, California where she worked first as an Executive Officer for the 412th Operations Group Commander. After a year, she moved to the 411th Flight Test Squadron to work as a Flight Test Engineer for the F-22 Raptor Program. In August 2011, she entered the Graduate Aeronautical Engineering program, School of Engineering, Air Force Institute of Technology to obtain a Master's Degree in aeronautical engineering. Upon graduation, Captain Drumm will be assigned to the Air Force Research Laboratory, Wright-Patterson Air Force Base, Ohio.

REPORT DOCUMENTATION PAGE

Form Approved
OMB No. 0704–0188

1. REPORT DATE *(DD–MM–YYYY)*	2. REPORT TYPE	3. DATES COVERED *(From — To)*
21–03–2013	Master's Thesis	Aug 2011 — Mar 2013

4. TITLE AND SUBTITLE

Computational Simulation of Explosively Generated Pulsed Power Devices

5a. CONTRACT NUMBER

5b. GRANT NUMBER

5c. PROGRAM ELEMENT NUMBER

6. AUTHOR(S)

Drumm, Mollie C., Capt, USAF

5d. PROJECT NUMBER

5e. TASK NUMBER

5f. WORK UNIT NUMBER

7. PERFORMING ORGANIZATION NAME(S) AND ADDRESS(ES)

Air Force Institute of Technology
Graduate School of Engineering and Management (AFIT/EN)
2950 Hobson Way
WPAFB OH 45433-7765

8. PERFORMING ORGANIZATION REPORT NUMBER

AFIT-ENY-13-M-11

9. SPONSORING / MONITORING AGENCY NAME(S) AND ADDRESS(ES)

United States Army Aviation and Missile Research, Development, and Engineering Center
Redstone Arsenal, Huntsville, AL 35898-5000
COMM 256-842-5131
Attn: Allen H. Stults
Email: allen.h.stults.civ@mail.mil

10. SPONSOR/MONITOR'S ACRONYM(S)

AMRDEC

11. SPONSOR/MONITOR'S REPORT NUMBER(S)

12. DISTRIBUTION / AVAILABILITY STATEMENT

APPROVED FOR PUBLIC RELEASE; DISTRIBUTION UNLIMITED.

13. SUPPLEMENTARY NOTES

14. ABSTRACT

Technology and size constraints have limited the development of the end game mechanisms of today's modern military weapons. A smaller, more efficient means of powering these devices is needed, and explosive pulsed power devices could be that answer. While most prior research has been in the experimental field, there is a need for more theory-based research and a computer modeling capability. The objective of this research was to use experimental data collected by the US Army at Redstone Arsenal from their ferroelectric generator (FEG) design in combination with the ALEGRA-EMMA code to develop a computer model that can accurately represent an FEG and that can be verified against experimental data and used to predict future experiments. While the ALEGRA code is not capable of simulating the breakdown phenomenon seen in the open circuit cases, the model can accurately reproduce the peak values for the current but has problems reproducing the peak values for the voltage. Overall, the developed model provides a good baseline simulation capability that can be used as a springboard for future development with further research.

15. SUBJECT TERMS

Computer Simulation, Hydrocode, Pulsed Power Generation

16. SECURITY CLASSIFICATION OF:			17. LIMITATION OF ABSTRACT	18. NUMBER OF PAGES	19a. NAME OF RESPONSIBLE PERSON
a. REPORT	b. ABSTRACT	c. THIS PAGE			Dr. Robert Greendyke, AFIT/ENY
U	U	U	U	105	19b. TELEPHONE NUMBER *(include area code)* (937) 255-3636, x4567; robert.greendyke@afit.edu